Improved Multi-Ended Impedance-Based Fault Locating for Untransposed Transmission Lines

Sathish Kumar Mutha, Arun Shrestha, and Sajal Harmukh, *Schweitzer Engineering Laboratories, Inc.*

***Abstract*—Impedance-based fault-locating algorithms come in three types: single-ended, multi-ended using remote currents, and multi-ended using both remote currents and voltages. The choice of the method depends on the available signals. The traditional algorithms often assume that transmission lines are perfectly transposed when, in fact, all lines are either untransposed or not perfectly transposed. This assumption affects the accuracy of these methods. This paper presents a practical method to estimate sequence-coupling parameters of transmission lines using local and remote current and voltage data. Using the estimated parameters, a new multi-ended impedance-based fault-location algorithm is proposed, which provides improved fault-locating accuracy for untransposed lines. The paper also provides simulations and field cases results, which demonstrate the efficacy of the proposed method.**

I. Introduction

Fault locating (FL) is an important aspect of protective relaying. Accurate fault location is vital for quick and economical restoration of power. FL algorithms have evolved significantly over the years. While impedance-based FL algorithms have existed in relays for a long time, traveling-wave (TW)-based FL algorithms have been implemented more recently in relays [1], which provide exceptionally accurate fault location. However, TWs are not always launched, and the accuracy of TW-based FL depends on whether it is multi-ended (ME) or single-ended (SE) [2]. This is the reason impedance-based FL algorithms are still pertinent today. Impedance-based FL can also be SE or ME. Further, the ME method can use either only remote currents [3] or both remote currents and voltages [4]. SE methods are prone to system non-homogeneity (different line and source angles) and unbalanced line loading. In SE methods, system non-homogeneity can lead to errors in fault-location estimation, particularly when fault resistance is present. ME methods are more effective at addressing errors due to fault resistance. However, traditional ME algorithms still face challenges with accuracy due to unbalanced line loading. The ME method, using remote currents, relies on one-end faulted-loop voltages and total fault currents. Their accuracy depends on correct faulted-loop identification and the proper application of the zero-sequence compensation factor (k0). The ME method, using both remote currents and voltages, however, uses the negative-sequence network and does not depend on faulted-loop identification or k0 factor, making it a more robust and accurate FL method [5]. More recently, some ME methods have been proposed that use remote data (either synchronized or unsynchronized) to estimate line parameters, Zc (characteristic impedance of the line per unit length) and γ (propagation constant), as well as to determine fault location [6]. They make use of long-line equations in positive-sequence networks to estimate both, Zc and γ, and to locate faults. However, the long-line equations can only be applied in cases of transposed lines where each of the sequence networks, in the pre-fault state, are decoupled from each other. In an untransposed line, sequence networks are coupled, and long-line equations cannot be applied accurately. The authors have previously proposed a ME impedance-based FL algorithm, which uses incremental sequence quantities [7]. This method provides a better fault-location estimate by removing the impact of load current. However, the method does not account for the coupling of sequence quantities in the pure-fault network.

Existing ME methods assume a transposed line while estimating the fault location. However, all lines are either untransposed or not perfectly transposed for economic and practical limitations [8] [9]. The use of existing methods with the transposed assumption of an untransposed line leads to errors in the estimated fault location. Untransposed lines exhibit unequal mutual-coupling line parameters between different phases. Consequently, in the sequence domain, this results in nonzero-sequence-coupling parameters, meaning that the off-diagonal terms in the sequence impedance matrix (Z_{012}) are nonzero. In the absence of these untransposed line parameters, it is difficult to accurately determine the fault location. To improve accuracy in the ME method that utilizes remote currents and voltages, we present a novel approach in this paper; first, to accurately determine the sequence-coupling parameters using pre-fault data, and second, to use the estimated sequence-coupling parameters to accurately determine the fault location for unbalanced faults. For balanced faults, the lack of line transposition does not significantly affect the fault-location estimation (see Section II) and the traditional methods work well.

The paper is organized as follows: Section II provides the background on untransposed errors (ME FL errors due to lack of line transpositions) for single-circuit and double-circuit lines. Section III provides the proposed FL algorithm. Section III also provides an error analysis of the proposed approach as applied to double-circuit lines. Section IV provides the comparison results using simulations and field events. Section V provides the limitations. Derivations are included in the Appendices.

II. Background on Untransposed Errors

In this section, we explore fault-location estimation errors caused by untransposed line parameters when they are not accounted for in the FL method. Fig. 1 shows the single-line

diagram of an untransposed transmission line with an unbalanced fault at a location of m per unit from the sending end, S.

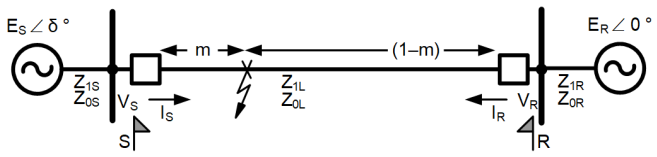

Fig. 1 Single-line diagram of a faulted transmission line.

The sequence network equation for this two-source power system under normal operating conditions is given in (1).

$$\begin{bmatrix} V_{0S} - V_{0R} \\ V_{1S} - V_{1R} \\ V_{2S} - V_{2R} \end{bmatrix} = \begin{bmatrix} Z_{00} & Z_{01} & Z_{02} \\ Z_{10} & Z_{11} & Z_{12} \\ Z_{20} & Z_{21} & Z_{22} \end{bmatrix} \bullet \begin{bmatrix} I_{0S} \\ I_{1S} \\ I_{2S} \end{bmatrix} \quad (1)$$

Where:

0, 1, or 2 = Zero-, positive-, or negative-sequence quantity; respectively (denoted by variable [q] henceforth).

$V_{[q]S/R}$ = [q]th sequence sending-/receiving-end voltage.

$I_{[q]S}$ = [q]th sequence sending-end current.

$Z_{[q1][q2]}$ = Sequence impedance coupling from q2 sequence network to q1 sequence network.

For an unbalanced fault (shown in Fig. 1) the sequence network can be written as shown in (2):

$$\begin{bmatrix} V_{0Sf} - V_{0Rf} \\ V_{1Sf} - V_{1Rf} \\ V_{2Sf} - V_{2Rf} \end{bmatrix} = m \bullet \begin{bmatrix} Z_{00} & Z_{01} & Z_{02} \\ Z_{10} & Z_{11} & Z_{12} \\ Z_{20} & Z_{21} & Z_{22} \end{bmatrix} \bullet \begin{bmatrix} I_{0Sf} \\ I_{1Sf} \\ I_{2Sf} \end{bmatrix} - (1-m) \bullet \begin{bmatrix} Z_{00} & Z_{01} & Z_{02} \\ Z_{10} & Z_{11} & Z_{12} \\ Z_{20} & Z_{21} & Z_{22} \end{bmatrix} \bullet \begin{bmatrix} I_{0Rf} \\ I_{1Rf} \\ I_{2Rf} \end{bmatrix} \quad (2)$$

Where:

f subscript refers to faulted quantities.

m is the per-unit fault location from the sending end.

$I_{[q]Rf}$ is the [q]th sequence receiving-end current.

It is important to note that (2) is derived by equating the fault-point voltage calculations from both line ends, under the assumption that the voltage and current measurements are time-synchronized. When the measurements from both ends are synchronized, fault resistance becomes irrelevant. Conversely, if the signals are not time-synchronized, (2) may not be applicable. In such cases, unsynchronized phasor fault-locating methods [8] can be used, though variations in fault resistance might introduce additional errors.

Extracting the negative-sequence network equation from (2) (the last row), we have:

$$V_{2Sf} - V_{2Rf} = \mathrm{m}(Z_{20}I_{0\mathrm{Sf}} + Z_{21}I_{1\mathrm{Sf}} + Z_{22}I_{2\mathrm{Sf}}) - (1-\mathrm{m})(Z_{20}I_{0\mathrm{Rf}} + Z_{21}I_{1\mathrm{Rf}} + Z_{22}I_{2\mathrm{Rf}}) \quad (3)$$

Traditional approaches assume a transposed line and further assume that the sequence-coupling parameters Z_{21} and Z_{20} are zero. This assumption simplifies (3) as:

$$V_{2Sf} - V_{2Rf} = \mathrm{m} \bullet Z_{22} \bullet I_{2\mathrm{Sf}} - (1-\mathrm{m}) \bullet Z_{22} \bullet I_{2\mathrm{Rf}} \quad (4)$$

Solving this simplified equation for m, we get

$$m = real\left(\frac{V_{2Sf} - V_{2Rf} + Z_{22} \bullet I_{2Rf}}{Z_{22} \bullet (I_{2Sf} + I_{2Rf})}\right) \quad (5)$$

It is important to note that Z_{11} and Z_{22} are equal, and both are equal to Z_{1L}, which is usually entered in the relay as a setting for the line parameter. The Z_{1L} value is obtained using the average values of self and mutual impedances.

A. Single Circuit—Untransposed Errors Analysis

Traditional ME fault-location estimation uses (5) and is referred to as the traditional approach. The measured faulted current consists of two parts, namely the load current and the pure-fault current. We can then write, using the superposition principle [10], the following for the negative-sequence network using (3)

$$\begin{aligned} V_{2Sf} - V_{2Rf} = {} & \mathrm{m}Z_{20}(I_{0\mathrm{S-FLT}} + \mathrm{I}_{0\mathrm{S-PRE}}) \\ & + \mathrm{m}Z_{21}(I_{1\mathrm{S-FLT}} + \mathrm{I}_{1\mathrm{S-PRE}}) \\ & + \mathrm{m}Z_{22}(I_{2\mathrm{S-FLT}} + \mathrm{I}_{2\mathrm{S-PRE}}) \\ & -(1-\mathrm{m})Z_{20}(I_{0\mathrm{R-FLT}} + \mathrm{I}_{0\mathrm{R-PRE}}) \\ & -(1-\mathrm{m})Z_{21}(I_{1\mathrm{R-FLT}} + \mathrm{I}_{1\mathrm{R-PRE}}) \\ & -(1-\mathrm{m})Z_{22}(I_{2\mathrm{R-FLT}} + \mathrm{I}_{2\mathrm{R-PRE}}) \end{aligned} \quad (6)$$

Where:

(-FLT) subscript refers to pure-fault current component of the faulted current.

(-PRE) subscript refers to load-current component of the faulted current.

Any voltage-drop term in (6) that is not part of (4) causes errors in fault-location estimates. For analysis purposes, these errors can be categorized as:

1. Load-current-based errors: As the name suggests, these errors are caused due to the load current part of the faulted current. Load current flows in one direction irrespective of the fault location. As such, it has a different effect on fault-location estimates compared to pure-fault currents, which flow opposite to each other from either line end, for an internal fault. In (6), there are four sequence-coupling voltage-drop terms due to load currents, which can be further grouped into the following two groups for the two sequence load currents, as shown in (7) and (8).

a) Positive-sequence load-current-based error: This is the voltage-drop error in the negative-sequence circuit due to positive-sequence load currents.

$$ErrLoad_{Pos} = mZ_{21}I_{1S-PRE} - (1-m)Z_{21}I_{1R-PRE}$$

$I_{1S\text{-}PRE}$ is approximately equal to $I_{1R\text{-}PRE}$, with the difference of the line charging current. For the ease of error analysis, this line charging current is ignored, which leads to the following, (7).

$$ErrLoad_{Pos} = Z_{21}I_{1S-PRE} \quad (7)$$

b) Zero-sequence load-current-based error: This is the voltage-drop error in the negative-sequence circuit due to zero-sequence load current.

$$ErrLoad_{Zero} = Z_{20} I_{0S-PRE} \quad (8)$$

2. Pure-fault current-based errors: These errors are caused due to the pure-fault current part of the faulted current. In (6), there are four such terms, which can be further grouped into the following two groups for two sequence fault currents, as shown in (9) and (10).

a) Positive-sequence pure-fault current-based error: This is the voltage-drop error in the negative-sequence circuit due to positive-sequence pure-fault currents.

$$ErrFLT_{Pos} = Z_{21}[mI_{1S-FLT} - (1-m)I_{1R-FLT}] \quad (9)$$

These two voltage drops, $mI_{1S\text{-}FLT}$ and $(1–m)I_{1R\text{-}FLT}$, oppose each other.

b) Zero-sequence fault current-based error: This is the voltage-drop error in the negative-sequence circuit due to zero-sequence currents.

$$ErrFLT_{Zero} = Z_{20}[mI_{0S-FLT} - (1-m)I_{0R-FLT}] \quad (10)$$

Equations (9) and (10) show that for a homogenous system with equal, local and remote, source-impedance ratios (SIRs) (the ratio of source impedance to the line impedance), if the fault is at 50 percent of the line, then the two voltage-drop terms, in (9) and (10), will perfectly cancel each other. Hence, the factors that affect the pure-fault current-based errors are

- SIR differences between the sending end and the receiving end
- Fault location

The same error analysis is extended to double-circuit lines in the next subsection.

B. Double Circuit—Untransposed Errors Analysis

In addition to errors listed in (7) through (10), a double-circuit line has additional mutual-coupling errors coming from the parallel line's positive-, negative-, and zero-sequence currents. The complete list of errors, List 1, for an end-to-end parallel line, is shown below (the derivation is in Appendix G).

1. $Z_{21} \bullet [\mathrm{m} \bullet I_{1\mathrm{S-FLT}} - (1-\mathrm{m}) \bullet I_{1\mathrm{R-FLT}}]$
2. $Z_{21} \bullet [I_{1\mathrm{S-PRE}}]$
3. $Z_{2-1\mathrm{P}} \bullet [I_{1\mathrm{SP-FLT}}]$
4. $Z_{2-1\mathrm{P}} \bullet [I_{1\mathrm{SP-PRE}}]$
5. $Z_{20} \bullet [\mathrm{m} \bullet I_{0\mathrm{S-FLT}} - (1-\mathrm{m}) \bullet I_{0\mathrm{R-FLT}}]$
6. $Z_{20} \bullet [I_{0\mathrm{S-PRE}}]$
7. $Z_{2-0\mathrm{P}} \bullet [I_{0\mathrm{SP-FLT}}]$
8. $Z_{2-0\mathrm{P}} \bullet [I_{0\mathrm{SP-PRE}}]$
9. $Z_{2-2\mathrm{P}} \bullet [I_{2\mathrm{SP-FLT}}]$
10. $Z_{2-2\mathrm{P}} \bullet [I_{2\mathrm{SP-PRE}}]$

List 1. Untransposed error terms for parallel lines with the traditional approach. (Subscript P refers to the quantities from the parallel line.)

There can be other kinds of parallel lines [11], which are not covered in the paper.

In the next subsection, several simulation results are presented to illustrate the impact of untransposed errors in traditional ME FL for a single-circuit untransposed line. These results are compared with those from traditional ME FL for a transposed line.

C. Single-Circuit Test Results—Traditional Approach

This section illustrates the impact of the traditional FL accuracy for an untransposed line. Equation (5) is applied for unbalanced faults; and the positive-sequence approach mentioned in [7] is applied for balanced faults. We have used a single-circuit 400 kV, 100 km line with a horizontal tower configuration (line parameter details are provided in the Appendix (Table IV and Table V). The line is analyzed under two scenarios: one where it is fully transposed, and another where it is left untransposed. Various fault conditions were applied to compare the accuracy differences between the transposed and untransposed cases. The single-line diagram of the tested system is shown in Fig. 1.

The test cases were selected to demonstrate the impact of different power system conditions on the untransposed errors, as discussed in Subsection A. We analyzed the same line under load-current-based untransposed errors, (7) and (8), and pure-fault current-based untransposed errors, (9) and (10), separately by changing one parameter at a time to compare results. The traditional approach on transposed lines does not exhibit untransposed errors and thus provides a reference for fault-location accuracy in untransposed scenarios.

First, to investigate the load errors in the untransposed errors, we kept the sending-end SIR_S and the receiving-end SIR_R the same and chose a fault location at 50 percent of the line length. The choice of these parameters removes the pure-fault error as discussed previously.

Fig. 2 provides the results for fault-location estimates when only loading is varied. When the load is minimum (one degree load angle is chosen here), the effects of (7) and (8) are also minimum. Hence, from Fig. 2b, we can see that transposed and untransposed lines both have almost equal fault-location accuracy for all the fault types.

When the line loading is increased to ± 20 degrees, load-current-based errors increase. This, in turn, increases the fault-location errors, as can be seen in Fig. 2a and Fig. 2c. We can also see that the transposed line FL is not affected by these load-current conditions.

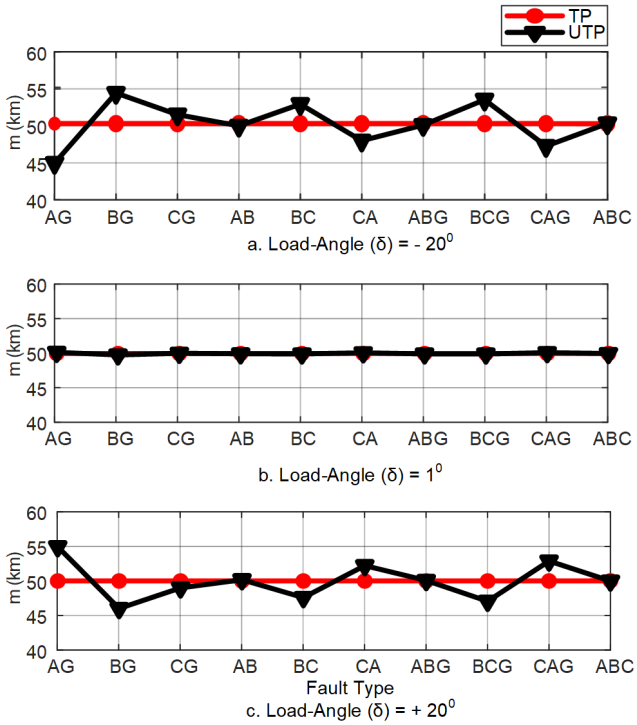

Fig. 2. Horizontal tower configuration, 400 kV system, line length (LL) = 100 km, SIR_S = 1, SIR_R = 1, fault location = 50 km, Rf = 40 ohms, varying load conditions (TP = Transposed; UTP = Untransposed).

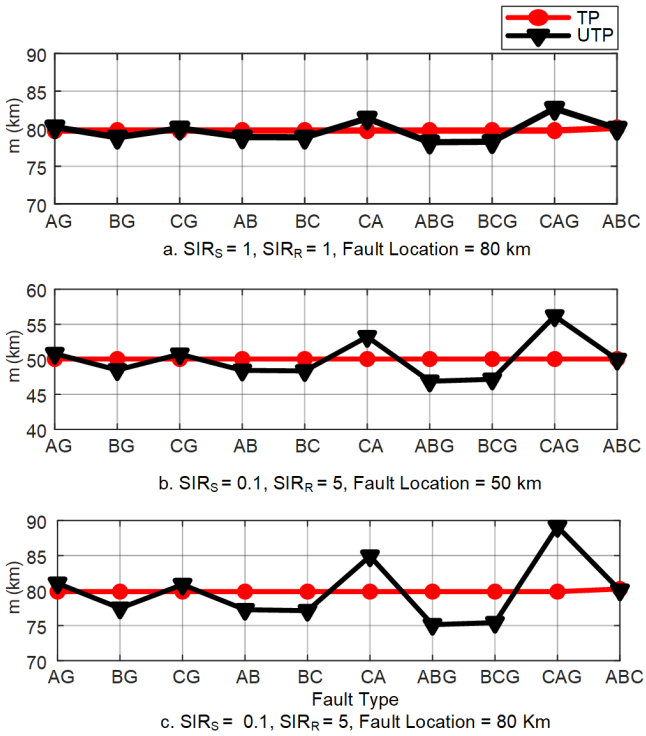

Fig. 3. Horizontal tower configuration, 400 kV system, LL = 100 km, load angle = 1 degree, Rf = 40 ohms, varying SIR or fault-location conditions. (TP = Transposed; UTP = Untransposed)

Next, to investigate the effect of pure-fault current-based errors, pre-fault load is fixed at minimum load flow, i.e., at one degree. The SIR difference and fault location are varied individually at first, and then both are varied simultaneously.

The local and remote SIR angles were kept fixed so that the source impedances were

$$Z_{xS} = Z_{xL} \bullet (SIR_S \angle -5^0)$$
$$Z_{xR} = Z_{xL} \bullet (SIR_R \angle -8^0) \quad (11)$$

Where x = 0, 1.

In the case shown in Fig. 3a, the SIR_S and SIR_R magnitudes are fixed at one, and the fault location is changed to 80 percent of the line length. We can see the increase in errors for untransposed lines. This increase is due to the unequal sequence mutual-coupling voltage drop in the line on either side of the fault location, as the simulation is not symmetric, unlike the fault location, which is at the midpoint (50 km) of the line. This can be understood from (9) and (10).

Fig. 3b analyzes the effect of SIR difference on untransposed errors. Here, the pre-fault load angle is maintained at one degree and fault location is kept at the midpoint of the line. This setup isolates the pure-fault current errors, which arise due to the different fault current contributions from the two ends. Fig. 3c shows the combined effects of SIR difference and fault location on the increase in errors. Again, the lack of symmetry in the faulted line leads to increased untransposed errors, as illustrated by (9) and (10), due to the unequal sequence mutual-coupling voltage present on either side of the fault point.

These results illustrate the effects of individual untransposed error contributors. The combined effect of these individual contributors to the untransposed errors are tested separately, and the results (for only untransposed lines) are provided in Section IV.

While the traditional approach on transposed lines remains unaffected by any of the discussed power system operating conditions, the traditional approach on untransposed lines is impacted due to the neglect of the sequence mutual-coupling line parameters, Z_{21} and Z_{20}, in the negative-sequence network. Hence, to address the untransposed errors, we need to include these line parameters in the FL algorithm. In the next section, we provide the details for estimating and including these line parameters in the FL algorithm. This way, the user does not have to provide additional line parameter data to get more accurate fault-location estimates.

III. Proposed Fault-Locating Algorithm

The proposed FL method uses the negative-sequence network because it is not influenced by source voltages, charging currents, and varying parameters based on the weather conditions. The method provides improved fault-location estimates for unbalanced faults, i.e., SLG, LL, and LLG faults. For balanced faults, both the traditional approaches—positive-sequence and average of three phase-phase equations' estimates—are adequate for addressing untransposed line errors. Refer to FL accuracy on untransposed lines for ABC fault results in Section II.

It was shown in Section II that ignoring the Z_{21} and Z_{20} components is the primary cause of errors in fault-location algorithms based on negative-sequence quantities for unbalanced faults. To address this, the proposed fault-locating method first estimates the sequence mutual-coupling line parameters in the negative-sequence network (Z_{21} and Z_{20}). These parameters are then used in the negative-sequence network to accurately estimate the fault location.

The estimation of sequence-coupling parameters is shown in Subsection A, while their use in network equations for accurate fault estimation is shown in Subsection B. Subsection C discusses some considerations for parallel lines.

A. Z_{21} and Z_{20} Estimation

In an untransposed line, the sequence networks are coupled through electromagnetic and electrostatic links during the pre-fault state. Fig. 4 shows the lumped-parameter nominal pi-circuit representation of sequence networks in the pre-fault state. The line also presents the shunt admittances, which can be represented as shown below, in a similar way as (1).

$$[I_{012}] = [Y_{012}][V_{012}] \tag{12}$$

The flow of current in the negative- and zero-sequence networks are representations of the natural unbalance due to the asymmetry in line geometry. The unbalance in power systems comes mainly from lines. The electromagnetic coupling between the networks is represented as current-dependent voltage sources while the electrostatic coupling is represented as voltage-dependent current sources. Fig. 4 is used as a reference to derive the sequence-coupling parameters. The quantities and parameters in Fig. 4 will be described in the different steps of the parameter estimation.

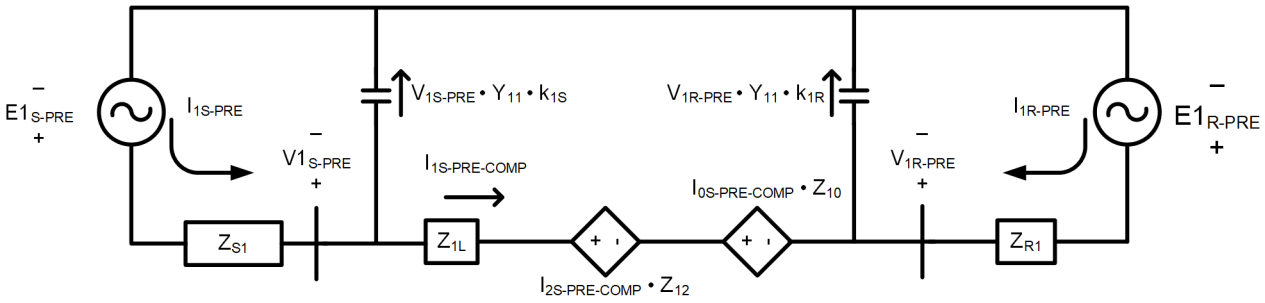

a) Positive-Sequence Pre-Fault Network

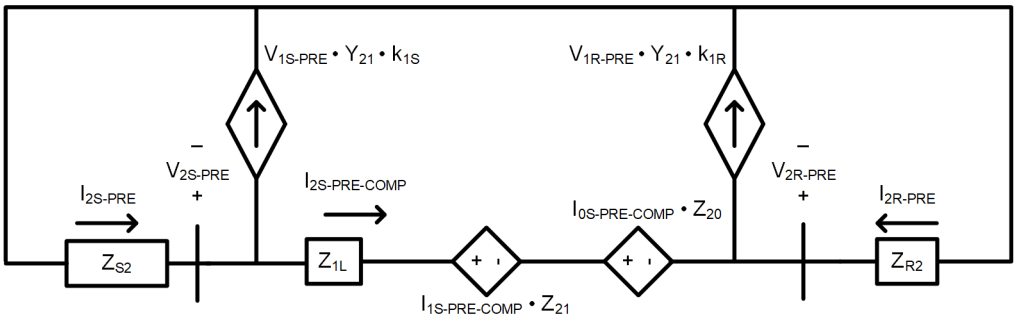

b) Negative-Sequence Pre-Fault Network

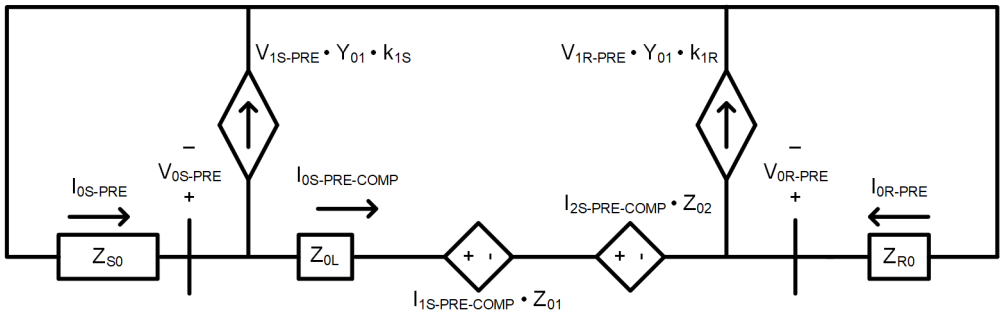

c) Zero-Sequence Pre-Fault Network

Fig. 4. Pre-fault sequence network diagrams.

The estimation of sequence-coupling parameters for the negative-sequence circuit is done in three steps: estimation of positive-sequence admittance-coupling parameters, compensation of the sequence currents to remove positive-sequence voltage-based capacitive currents, and estimation of sequence-coupling impedances. These steps are described in more detail below.

1. Estimation of admittance line parameters:

   The sequence admittance-coupling parameters Y_{01} (the admittance coupling from the positive-sequence to the zero-sequence network), Y_{11} (positive-sequence self-admittance), and Y_{21} (the admittance coupling from the positive-sequence to the negative-sequence network) are estimated using (15), (16), and (17). Only the positive-sequence admittance-coupling parameters are considered for all three networks given the fact that positive-sequence voltage is much higher than other sequence voltages during the pre-fault state.

   In Fig. 4, k_{1S} and k_{1R} refer to the admittance distribution factors, which take into account unequal voltage magnitudes at the two ends and their relative contribution to the charging current. Here, k_{1S} and k_{1R} describe what percentage (per unit) of the sum of the two voltages is the local voltage, with the results expressed as absolute values. They can be found as shown in (13).

$$k_{1S} = \left|\frac{V_{1S-PRE}}{V_{1S-PRE} + V_{1R-PRE}}\right|$$
$$k_{1R} = \left|\frac{V_{1R-PRE}}{V_{1S-PRE} + V_{1R-PRE}}\right| \quad (13)$$

   Once k_{1S} and k_{1R} are known, we can write (using the pi model approach) the following for the positive-sequence network charging current,

$$I_{1S-PRE} + I_{1R-PRE} = k_{1S} \bullet Y_{11} \bullet V_{1S-PRE} + k_{1R} \bullet Y_{11} \bullet V_{1R-PRE} \quad (14)$$

   which can then be simplified to obtain Y_{11}, total shunt admittance, as shown in (15).

$$Y_{11} = \frac{I_{1S-PRE} + I_{1R-PRE}}{k_{1S} \bullet V_{1S-PRE} + k_{1R} \bullet V_{1R-PRE}} \quad (15)$$

   A similar approach can be followed for pre-fault negative- and zero-sequence networks to obtain Y_{21} and Y_{01} as shown in (16) and (17).

$$Y_{21} = \frac{I_{2S-PRE} + I_{2R-PRE}}{k_{1S} \bullet V_{1S-PRE} + k_{1R} \bullet V_{1R-PRE}} \quad (16)$$

$$Y_{01} = \frac{I_{0S-PRE} + I_{0R-PRE}}{k_{1S} \bullet V_{1S-PRE} + k_{1R} \bullet V_{1R-PRE}} \quad (17)$$

2. Compensation of sequence currents to remove capacitive-coupling current from positive-sequence voltage:

   The sequence currents from each end are compensated to remove the respective end's capacitive-charging current resulting from positive-sequence voltage. This improves the estimation of sequence current flowing in the line. Equation (18) shows how the currents are compensated.

$$I_{1S-PRE-COMP} = I_{1S-PRE} - Y_{11} \bullet k_{1S} \bullet V_{1S-PRE}$$
$$I_{2S-PRE-COMP} = I_{2S-PRE} - Y_{21} \bullet k_{1S} \bullet V_{1S-PRE}$$
$$I_{0S-PRE-COMP} = I_{0S-PRE} - Y_{01} \bullet k_{1S} \bullet V_{1S-PRE} \quad (18)$$

3. Estimation of sequence-coupling impedances, Z_{21} and Z_{20}:

   Using Kirchoff's voltage law in Fig. 4b, the negative-sequence network (the sequence mutual-coupling impedance from positive-sequence to negative-sequence network), Z_{21}, can be estimated as shown in (19).

$$Z_{21} = \frac{V_{2S-PRE} - V_{2R-PRE} - Z_{IL} \bullet I_{2S-PRE-COMP}}{I_{1S-PRE-COMP}} \quad (19)$$

   Here, the term $\left(\frac{I_{0S-PRE-COMP} \bullet Z_{20}}{I_{1S-PRE-COMP}}\right)$ electromagnetic coupling from the zero-sequence network, is ignored. This is because, typically, the zero-sequence current is in the order of one percent of positive-sequence currents in normal power system operating conditions. Additionally, the magnitude of Z_{20} will be in the same range as Z_{21}. Therefore, the omission of this term results in only minor errors in the Z_{21} estimation. The magnitude of this error can be observed in Section IV.

   Using Kirchoff's voltage law in Fig. 4c, zero-sequence network (the sequence mutual-coupling impedance from the positive-sequence to the zero-sequence network), Z_{01}, can be estimated as shown in (20).

$$Z_{01} = \frac{(V_{0S-PRE} - V_{0R-PRE} - Z_{0L} \bullet I_{0S-PRE-COMP})}{I_{1S-PRE-COMP}} \quad (20)$$

   Here, the term $\left(\frac{I_{2S-PRE-COMP} \bullet Z_{02}}{I_{1S-PRE-COMP}}\right)$ electromagnetic coupling from negative-sequence network, is ignored. This is because, typically, the negative-sequence current is in the order of 2 to 4 percent of positive-sequence currents in normal power system operating conditions, and the magnitude of Z_{02} will be in the same range of Z_{01}. Therefore, the omission of this term results in only minor errors in the Z_{01} estimation. The magnitude of this error can be observed in Section IV.

   The sequence impedance matrix, $[Z_{012}]$, is not a symmetrical matrix. However, it does follow some symmetry, with Z_{01} equal to Z_{20} and Z_{10} equal to Z_{02} (see Appendix A). Thus, the calculation of Z_{01} also gives us Z_{20}, i.e., (21).

$$Z_{20} = Z_{01} \quad (21)$$

   Theoretically, the estimations we discussed for Z_{21} and Z_{20} do not change much with the load conditions (refer to simulation results in Section IV). However, it is preferred to estimate them close to higher load conditions when CT errors are smaller. A qualifying minimum load can be used to trigger the estimation of these parameters, which can be performed at regular intervals to account for any possible variation in zero-sequence related parameters, which may vary due to change in ground resistivity and other factors. In this paper, we use the pre-fault load, irrespective of its magnitude, to estimate Z_{21} and Z_{20}.

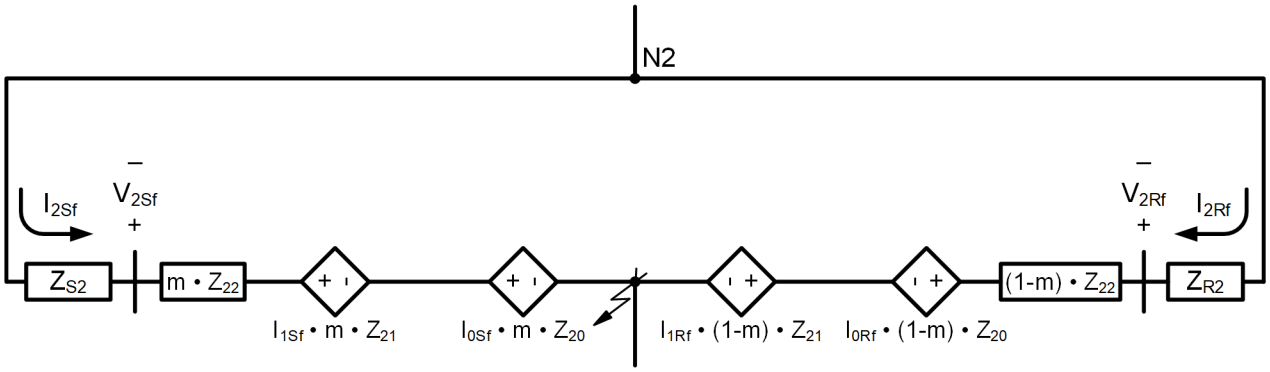

Fig. 5. Faulted negative-sequence network.

$$m = real\left(\frac{V_{2Sf} - V_{2Rf} + Z_{22} \bullet I_{2Rf} + Z_{21} \bullet I_{1Rf} + Z_{20} \bullet I_{0Rf}}{Z_{22} \bullet \left(I_{2Sf} + I_{2Rf}\right) + Z_{21} \bullet \left(I_{1Sf} + I_{1Rf}\right) + Z_{20} \bullet \left(I_{0Sf} + I_{0Rf}\right)}\right) \tag{22}$$

B. Fault-Location Estimation

As discussed earlier, Z_{21} and Z_{20} are used to represent the electromagnetic coupling due to I_1 and I_0, respectively, as current-dependent voltage sources in the negative-sequence network (see Fig. 5).

While working on pre-fault sequence networks for estimating Z_{21} and Z_{20}, admittance coupling from the positive-sequence network on all three networks is included. However, for faulted networks, we ignore the admittance coupling to keep the calculations simpler and more efficient.

Equation (22) provides the estimated fault location obtained by solving the network shown in Fig. 5, (see Appendix B for detailed derivation).

It is important to note that when Z_{21} and Z_{20} estimates are not available or if the line is transposed, we can simply substitute Z_{21} and Z_{20} with zero and (22) becomes identical to the traditional fault-location equation, as shown in (5).

C. Untransposed Parallel-Line Considerations

For untransposed parallel lines, there is sequence mutual coupling between the parallel lines in addition to the sequence coupling within each line. The following equation illustrates the relationship between the sequence networks of two parallel lines (L1 and L2) under normal power system operating conditions in the sequence domain.

$$\begin{bmatrix}[\Delta V_{012_{L1}}]\\ [\Delta V_{012_{L2}}]\end{bmatrix} = \begin{bmatrix}[Z_{012_{L1}}] & [Z_{012_{L12}}]\\ [Z_{012_{L21}}] & [Z_{012_{L2}}]\end{bmatrix}\begin{bmatrix}[I_{012_{L1S}}]\\ [I_{012_{L2S}}]\end{bmatrix}$$

$[\Delta V_{012_{Lx}}]$ = Line x sequence voltage drop, matrix

$[I_{012_{LxS}}]$ = Line x sending-end sequence currents, matrix

$[Z_{012_{Lx}}]$ = Line x sequence impedance, matrix

$[Z_{012_{Lxy}}]$ = Line y mutual sequence impedance on Line x, matrix

Where x, y = 1,2.

These additional sequence mutual-coupling terms from the parallel line play a role in Z_{21} and Z_{20} estimations. In this subsection, we propose an improved Z_{20} estimation for parallel lines, which accounts for zero-sequence mutual coupling between the circuits. Next, we analyze the errors in the estimations of Z_{21} and Z_{20}, as well as the errors in proposed fault-location estimation, when applied to parallel lines.

1) Improving Z_{20} Estimation for Untransposed Parallel Lines

Consider the single-line diagram of an end-to-end connected double-circuit line shown in Fig. 6. It illustrates that the two parallel lines share a common bus at either end. In Fig. 6, Z_{0M} refers to the zero-sequence mutual impedance between the two parallel lines. The zero-sequence coupling between the two circuits can be significant and needs to be accounted for in the Z_{20} estimation. It should be noted that the Z_{21} parameter is not affected significantly in the presence of a parallel line.

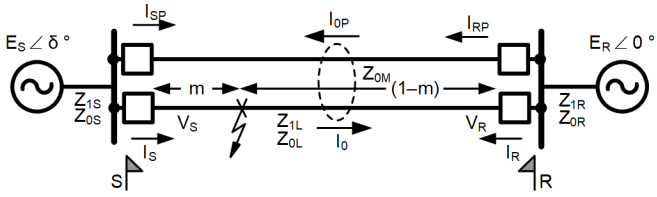

Fig. 6. Two-source power system model with parallel line.

Fig. 7 shows the pre-fault zero-sequence network of the line of interest for the system shown in Fig. 6. Recall that (20) and (21) from Section III.A demonstrate that Z_{20} is equal to Z_{01}, which is estimated from the zero-sequence network. It illustrates all the electromagnetic coupling from the parallel-line sequence networks as current-dependent voltage sources. In Fig. 6, currents with subscript P refer to parallel-line currents and parameters with subscript P refer to mutual-coupling parameter between the line of interest and the parallel line.

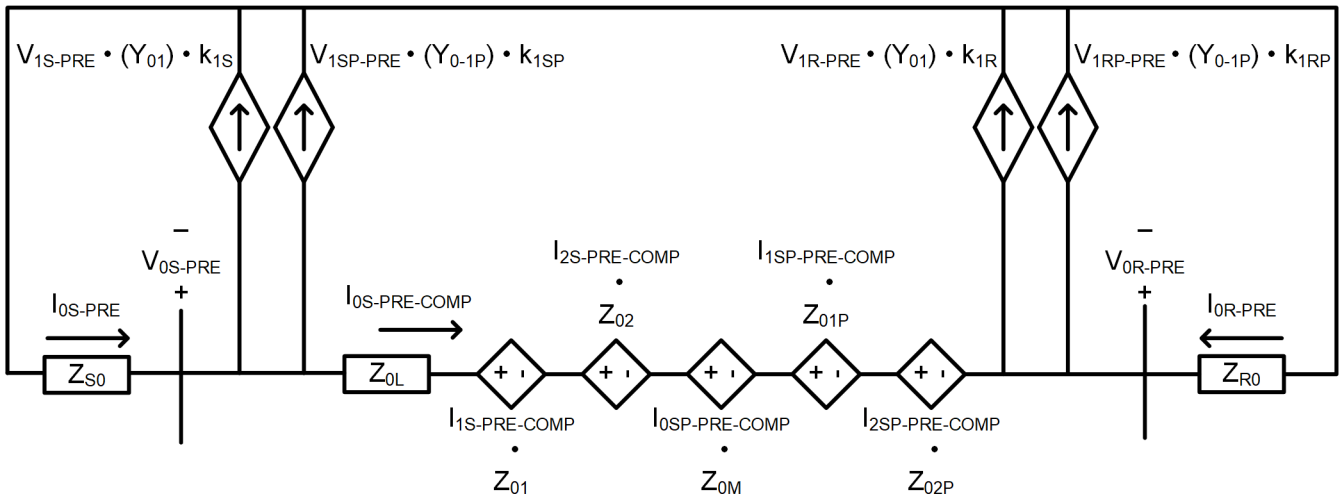

Fig. 7. Pre-fault zero-sequence network for a two-source power system with parallel line.

Because positive- and negative-sequence currents are balanced in nature, their net electromagnetic effect on a parallel line is low. However, zero-sequence current is not balanced and the net electromagnetic effect on the parallel line cannot be neglected [12]. Thus, we can ignore the mutual-coupling terms related to $Z_{0\text{-}1P}$ and $Z_{0\text{-}2P}$ (the impedance matrix example in the Appendix illustrates the validity of the assumption), while noting that we had already ignored the Z_{02} term when estimating Z_{20} in (20). However, even if the lines are fully transposed, Z_{0M} does not go away. With these assumptions, we can now write (23) for the zero-sequence network (in Fig. 7).

$$V_{0S-PRE} - V_{0R-PRE} = Z_{0L} \bullet I_{0S-PRE-COMP} + Z_{0M} \bullet I_{0SP-PRE-COMP} + Z_{01} \bullet I_{1S-PRE-COMP} \quad (23)$$

Looking at (23), we can note that the difference from the single-circuit case, (20), is the zero-sequence mutual-coupling term.

Further, we need to compensate the parallel-line zero-sequence current for capacitive current due to positive-sequence voltage in parallel line. Following the steps from Section III .A, we can write (24).

$$I_{0SP-PRE-COMP} = I_{0SP-PRE} - Y_{01} \bullet k_{1S} \bullet V_{1S-PRE} \quad (24)$$

The electrostatic coupling, due to positive-sequence voltage from the parallel line, $Y_{0\text{-}1P}$, is included in the Y_{01} estimation when using (17) (the derivation is in Appendix F). Therefore, no additional measures are required to account for $Y_{0\text{-}1P}$.

Z_{01} can then be estimated using (23).

$$Z_{01} = \frac{(V_{0S-PRE} - V_{0R-PRE} - Z_{0L} \bullet I_{0S-PRE-COMP} - Z_{0M} \bullet I_{0SP-PRE-COMP})}{I_{1S-PRE-COMP}} \quad (25)$$

Equation (25) provides a more accurate Z_{01} estimation than (20). Detailed comparison results between (20) and (25) are presented in Section IV.B. We refer to the (20)-based FL as the proposed approach, and to the (25)-based FL as the alternate approach.

2) *Analysis of Errors in Parameter Estimation and Fault-Location Estimation in Parallel Lines*

In this subsection, we dive deeper into the errors in parameter estimation and FL when applying the proposed method for the parallel lines.

In the previous subsection, we improved the Z_{20} estimation to include the parallel-line zero-sequence mutual-coupling effect. However, we did not change the Z_{21} estimation for the parallel-lines scenario. It can be shown that the Z_{21} estimated in case of parallel lines also includes the effect of positive-sequence current in the parallel line ($I_{1SP\text{-}PRE\text{-}COMP} \bullet Z_{2\text{-}1P}$) as it couples to the negative-sequence network (see (26)). There is also a negative-sequence current coupling from the parallel line to the line of interest. However, since parallel-line negative-sequence current is much smaller than parallel positive-sequence current in pre-fault condition, we ignore that effect.

Thus, the Z_{21} we estimate is effectively the sum of the true Z_{21} of the protected circuit and $Z_{2\text{-}1P}$ (parallel line I_{1P} coupling to the line-of-interest negative-sequence network). It should be noted that $Z_{2\text{-}1P}$ can be much smaller in comparison to Z_{21} because, as mentioned before, a positive-sequence current is a balanced current and produces almost no net flux as we move away from the line. However, since the two parallel lines are relatively close to each other, some coupling exists between I_{1P} and the line-of-interest negative-sequence network. A detailed derivation for (26) is provided in Appendix C. This Z_{21_eff} is an impedance estimation for parallel lines based on the pre-fault values, using (19), assuming equal currents in both lines.

$$Z_{21_{\text{eff}}} = Z_{21} + Z_{2-1P} \quad (26)$$

Similarly, while estimating Z_{01} using (25), we have not included the positive-sequence current effect from the parallel line ($I_{1SP\text{-}PRE\text{-}COMP} \bullet Z_{0\text{-}1P}$) in the zero-sequence network. Due to this, the effective estimated $Z_{01,}$ for parallel lines using the proposed approach, turns out to be as shown in (27). The derivation for (27) is provided in Appendix D. This $Z_{01\_eff\_new}$ is an impedance estimation based on the pre-fault values, assuming equal currents in both lines.

$$Z_{01\_eff\_new} = Z_{01} + Z_{0-1P} \quad (27)$$

Had we not improved the Z_{01} estimation for parallel-line zero-sequence mutual coupling to the line-of-interest zero-sequence network (Z_{0M}) using (25), the effective Z_{01} would have included the Z_{0M} effect as well. Equation (28) gives the effective Z_{01} when estimated using (20). See Appendix E for the derivation.

$$Z_{01\_eff\_old} = Z_{01} + Z_{0-1P} + Z_{0M} \bullet \frac{I_{0SP-PRE-COMP}}{I_{1S-PRE-COMP}} \quad (28)$$

Next, we analyze the errors in estimated fault location using the proposed approach for parallel lines. List 2 provides the list of errors, which result from the ignored impedances after the inclusion of effective Z_{21} and Z_{20} estimations, obtained from (26) and (27), in the faulted negative-sequence network (see Appendix H for more details).

1. $Z_{2-1P} \bullet [m \bullet I_{1S-FLT} - (1-m) \bullet I_{1R-FLT}]$
2. $Z_{2-1P} \bullet [I_{1SP-FLT}]$
3. $Z_{2-0P} \bullet [m \bullet I_{0S-FLT} - (1-m) \bullet I_{0R-FLT}]$
4. $Z_{2-0P} \bullet [I_{0SP-FLT}]$
5. $Z_{2-2P} \bullet [I_{2SP-FLT}]$
6. $Z_{2-2P} \bullet [I_{2SP-PRE}]$

List 2. Untransposed error terms for parallel lines with alternate approach.

In List 2, $I_{[q]SP-FLT}$ refers to the change in parallel-line pre-fault [q]th sequence current (pure-fault) because of a fault in the line of interest. For Errors 1 and 3, it should be recalled that the term $[m \bullet I_{xS-FLT} - (1-m) \bullet I_{xR-FLT}]$ (where x = 0, 1) has a self-deprecating nature, meaning the two terms have the same sign and tend to cancel each other out. When the sending-end and receiving-end source-impedance magnitudes and angles are the same and the fault is at 0.5 pu of the line length, they perfectly cancel each other out.

Here, we considered end-to-end parallel lines; however, for the other kinds of parallel lines, an error analysis should be run to identify more sources of error.

The next section shows the comparison results between the traditional approach and the proposed approach.

IV. Simulation and Field Event Results

This section provides the comparison results between the traditional approach (5) and proposed approach, (19) through (22), using phasor-based simulations for single-circuit lines with three different tower configurations, end-to-end parallel lines with two different tower configurations, and a few field events.

A. Single-Circuit Transmission Lines

The transmission line tower configuration and line parameters for each single-circuit line are provided in the Appendix (Table IV and Table V). For simplicity, the line length is fixed to 100 km. The source impedances are calculated as shown in (11). Fig. 8 shows the ideal Vs estimated Z_{21} (as per (19)) and estimated Z_{20}, as per (21), parameters for a 400 kV horizontal tower configuration with respect to load angle. Furthermore, Z_{20} shows slightly higher estimation error (5.5 percent) than Z_{21} (1.2 percent). The estimates do not change much with load angle variation. This is due to the inclusion of admittance compensation for pre-fault sequence currents (18) while estimating Z_{21} and Z_{20}. Next, we use these estimated line parameters for estimating the fault location.

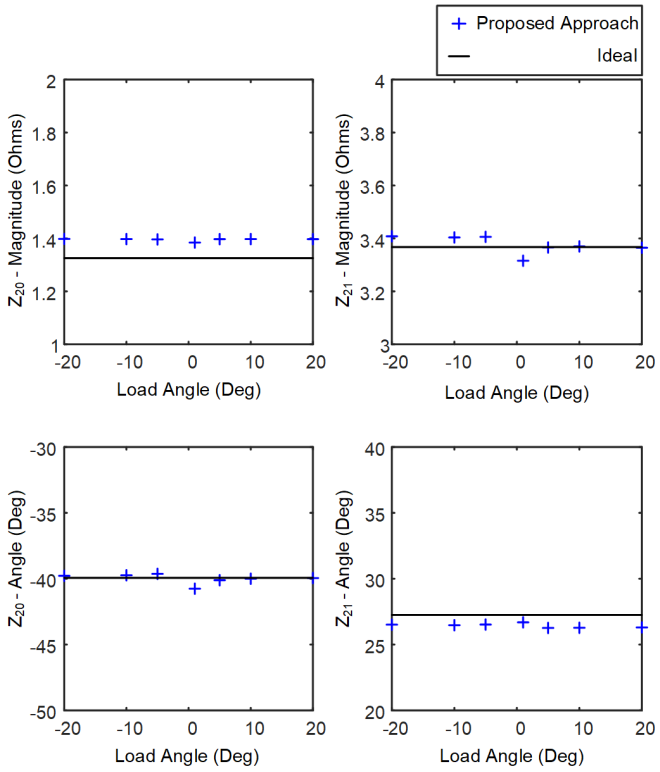

Fig. 8. Z_{20} and Z_{21} estimation for 400 kV horizontal tower configuration, $SIR_S = 0.1$, $SIR_R = 1$.

Fig. 9 shows the fault-location estimates from the traditional and proposed methods at 50 km fault location and three different load angles. As the SIR on both sides of the lines are equal and the fault is at the middle of the line, there are no pure-fault current-based errors. The fault-location estimate error in the traditional method is the result of not including load-current-based errors in its calculations. As the load angle increases, these errors increase, resulting in higher fault-location estimate errors in the traditional method. The fault-location estimates provided by the proposed method are close to the actual value as these errors are accounted for in the calculations.

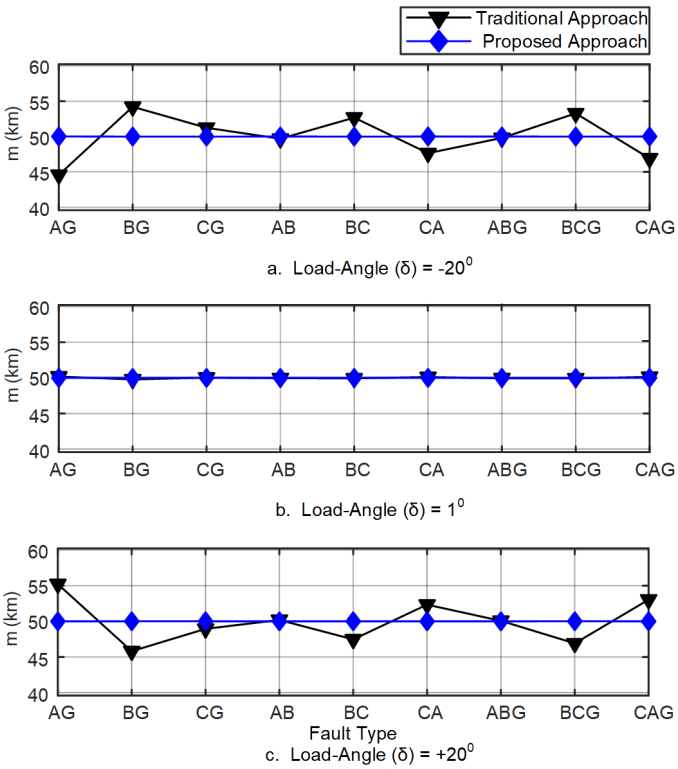

Fig. 9. Horizontal tower configuration, 400 kV system, LL = 100 km SIR_S = 1, SIR_R = 1, fault location = 50 km, Rf = 40 ohms.

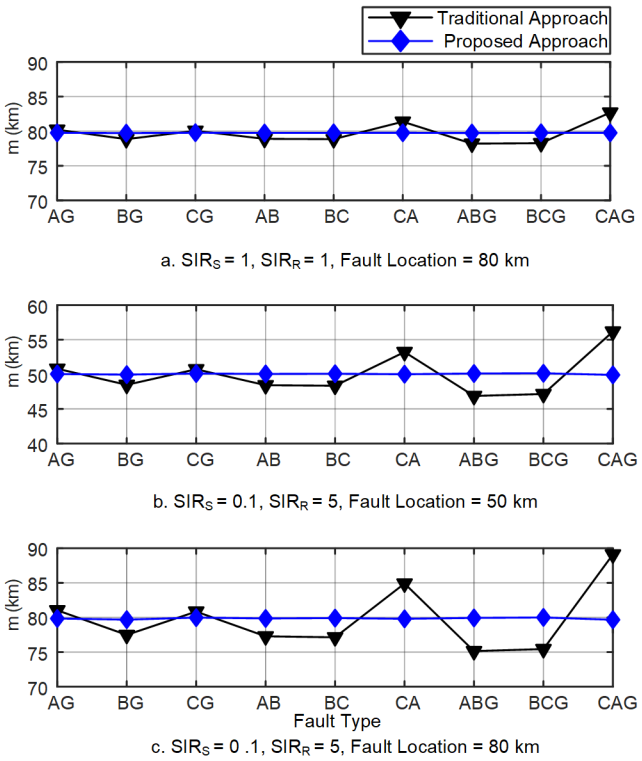

Fig. 10. Horizontal tower configuration, 400 kV system, LL = 100 km load angle = 1 degree, Rf = 40 ohms, varying SIR or fault-location conditions.

Next, we analyze the impact of pure-fault current-based error on the two methods. The load angle is kept low at one degree to minimize load-current-based errors. A zero-degree load angle is intentionally avoided because it prevents the estimation of Z_{21} and Z_{20} using the proposed method. This is due to (19) and (20), which have positive-sequence current in the denominator. Fig. 10 shows the fault-location estimates provided by the two methods for two different SIR conditions and two fault locations. The proposed method provides good fault-location estimates. The errors in traditional method fault-location estimates are due to not incorporating pure-fault current-based errors in its calculations.

So far, we analyzed the impact of load-current-based errors and pure-fault current-based errors separately in the traditional and the proposed methods. These errors result in poor fault-location estimates when the traditional method is used. As the proposed method accounts for these errors, the fault-location estimates are not affected by variation in load angle, SIR difference, or fault location. To test the efficacy of the proposed method, hundreds of faults are executed by varying fault locations, load angles, fault types, and fault resistance. Although fault resistance does not affect ME impedance-based FL methods, test cases with different fault resistance are considered to make the test coverage relevant to real-world scenarios.

The following variables are used for generating overall test cases.

Fault locations (km) = –> 30, 50, 80
Load angle (degree) = –> –20, –10, –5, 1, 5, 10, 20
Fault type = –> AG, BG, CG, AB, BC, CA, ABG, BCG, CAG
Fault resistance (ohms) = –> 0.001, 10, 40
SIR_S = –> 0.1
SIR_R = –>1, 1.5, 2, 2.5, 3, 3.5, 4, 4.5, 5

Fig. 11 shows the worst-case fault-location estimates provided by the traditional and proposed methods for each SIR_R by evaluating all combinations of the remaining variables mentioned previously. For the 400 kV horizontal tower configuration, the worst-case fault-location estimate error provided by the traditional method is 10.56 km, whereas it is 0.3259 km for the proposed method. Table I lists the fault-location estimates for three single-circuit tower configurations for various fault configurations discussed above. Compared to the traditional method, the proposed method estimates are within 1 to 2 tower spans. The test results prove the effectiveness of the proposed fault-location method for single-circuit lines.

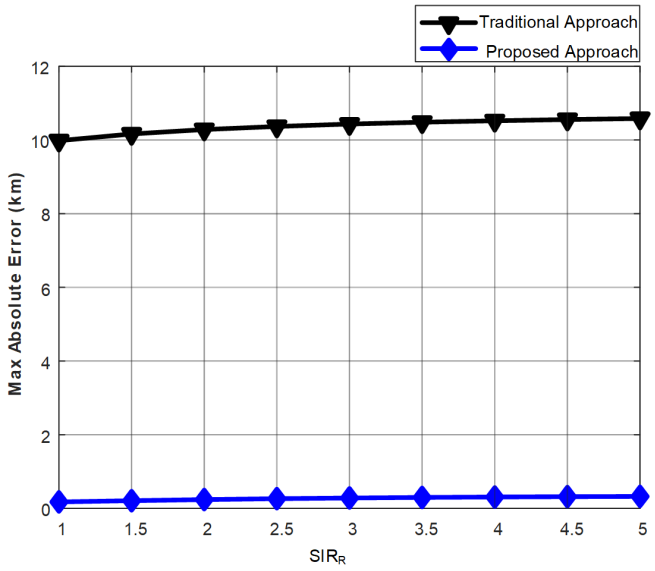

Fig. 11. Horizontal tower configuration, 400 kV system, $SIR_S = 0.1$.

TABLE I
WORST-CASE ABSOLUTE ERROR FOR VARIOUS TOWER CONFIGURATIONS

	Traditional Approach—Worst-case Error (km)	**Proposed Approach—Worst-case Error (km)**
400 kV Horizontal tower configuration	10.58	0.3259
400 kV Vertical tower configuration	12.1232	0.4215
230 kV Right angle tower configuration	7.348	0.3828

B. Double-Circuit Transmission Lines

This subsection presents simulation results for double-circuit untransposed lines using both the traditional (5) and proposed, (19) through (22), fault-locating approaches. Additionally, as discussed in Section III, we introduce an improved solution for Z_{20} (25) by incorporating parallel-line data. This section includes fault-locating results using an alternate approach where (20) in the proposed method is replaced with (25).

We considered an end-to-end parallel-line configuration for two different systems: one with a 230 kV double-circuit tower configuration and the other with a 400 kV double-circuit tower configuration. The single-line diagram for the test system is shown in Fig. 6. The transmission tower configuration and line parameters are provided in the Appendix (Table IV and Table V). The source impedances are calculated as shown in (11). For the proposed approach, Z_{21} and Z_{20} are first estimated before proceeding to estimate the fault location.

Fig. 12 shows the Z_{21} and Z_{20} estimates for both the proposed approach, (19) and (20), and the alternate approach, (25), for the 230 kV double-circuit configuration. The estimations were conducted at a fixed $SIR_S = 0.1 \angle -5^0$ and $SIR_R = 5 \angle -8^0$, across seven different load conditions. The accuracies of these estimates are compared against the ideal values $Z_{21}+Z_{2\text{-}1P}$ and $Z_{20} + Z_{2\text{-}0P}$, respectively. The rationale for this comparison is detailed in Section III.C.2. In contrast to single-circuit configurations, the estimation of Z_{20} in double-circuit configurations is influenced by loading conditions. However, the alternate approach shows that Z_{20} estimation is relatively unaffected by load variations, while Z_{21} estimation remains stable and meets expectations regardless of load conditions.

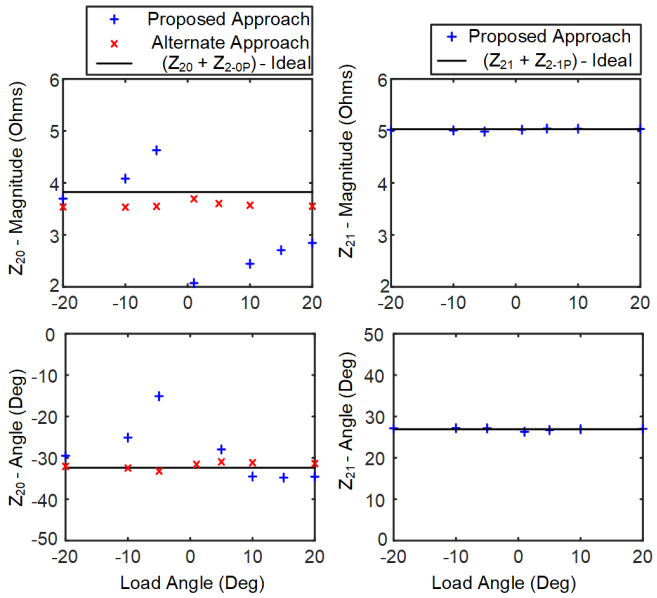

Fig. 12. Double-circuit, 230 kV system, $SIR_S = 0.1$, $SIR_R = 5$, Z_{21} and Z_{20} estimates at different loads.

It is evident that the proposed Z_{20} estimation, particularly its magnitude, is significantly affected by the load. Interestingly, higher loading conditions have contributed to improved accuracy in Z_{20} estimations. Now, let us see the effect of these estimations in FL.

The fault-location estimation comparison results for the 230 kV double-circuit line are shown in Fig. 13. The plot is generated by varying the SIR_R from 1 to 5 in increments of 0.5, while keeping SIR_S fixed at 0.1. The absolute maximum error (km) for various fault cases is recorded for each value of SIR_R. The power system variables for the test cases are as follows:

Fault locations (km) = –> 30, 50, 80
Load angle (deg) = –> –20, –10, –5, 1, 5, 10, 20
Fault type = –> AG, BG, CG, AB, BC, CA, ABG, BCG, CAG
Fault resistance (ohms) = –> 0.001, 10, 40

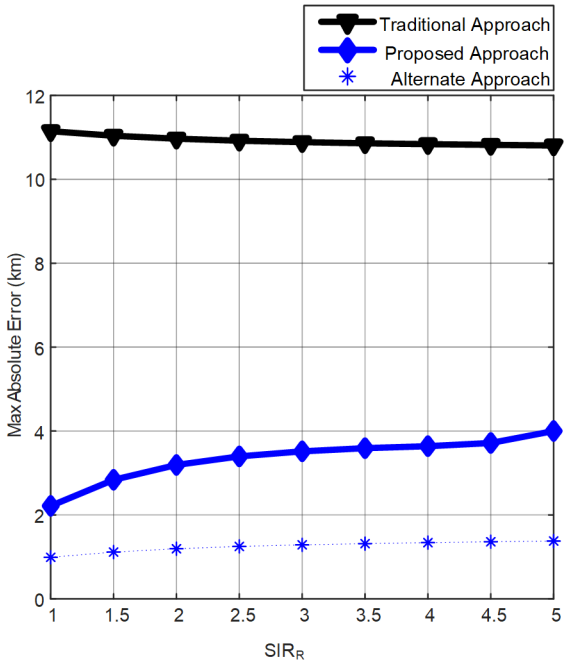

Fig. 13. Absolute maximum error comparison results for 230 kV double-circuit tower configuration, $SIR_S = 0.1$.

The plot in Fig. 13 shows that the proposed approach consistently provides accurate results overall, compared to the traditional method, despite lower load conditions affecting the Z_{20} estimation. One possible reason for this improvement is the effective reduction in Z_{21}-related untransposed errors.

Furthermore, fault-location estimation accuracy is further enhanced when incorporating Z_{01} from (25). However, this approach has a slight increase in errors with the increase in SIR_R. This trend can be explained through the error analysis presented in Section III.C, where Errors 1 and 3 from List 2. contribute to this reduction in accuracy. This is primarily due to the increase in differences between the pure-fault currents on the sending end and receiving end.

Table II presents the absolute maximum error values for two double-circuit configurations across various fault scenarios, as mentioned for Fig. 13.

TABLE II
WORST-CASE ABSOLUTE ERROR FOR DOUBLE-CIRCUIT LINES

	Traditional Approach—Worst-Case Error (km)	**Proposed Approach—Worst-Case Error (km)**	**Alternate Approach (Eq (25) based) Worst-Case Error (km)**
230 kV double-circuit tower configuration	11.15	4.0	1.38
400 kV double-circuit tower configuration	13.01	5.72	4.25

Table II demonstrates that the proposed approach shows consistent and substantial improvement, despite the inherent limitations of double-circuit lines.

The alternate approach for the 400 kV system has a worst-case error of 4.25 km at $SIR_S = 0.1$, $SIR_R = 5$, and fault location = 80 km. This higher error is due to Errors 1 and 3 from List 2.

C. *Field Events—Results*

To demonstrate the improved accuracy of the proposed FL method, we applied it to five field event reports, each with a known fault location. These events were processed using both traditional and proposed algorithms, and the comparison results are provided in Table III. For the proposed algorithm, pre-fault and fault data processing is done as shown [11].

Table III shows the fault type, pre-fault sequence currents, line parameters, and SIR. Source impedances are estimated from the available fault data (using relation, $Z_{2X} = -V_{2X}/I_{2X}$, where X=S for the sending end and R for the receiving end). Table III also provides the actual fault location determined by the field crew, the fault location estimated by the traditional FL algorithm, (5), and its error, the proposed method's Z_{21} and Z_{20} estimates, applying (18), (19), (20), and the fault location estimated by the proposed algorithm, (21), and its error. Below is more information on the field events:

- Field Event 1 is from a homogenous 115 kV line that is 33.63 km long with a few tap points. The pre-fault load was high, with pre-fault I_2 at 3.97 percent of I_1 and pre-fault I_0 at 0.16 percent of I_1. These values suggest that the traditional approach may introduce load-current-based untransposed errors, primarily due to I_2. Additionally, the SIR angles differ from each other and from the line angle, indicating non-homogeneity within the system. The fault was not located at the midpoint of the line, leading to further asymmetry. The system non-homogeneity and asymmetry can result in pure-fault current-based untransposed errors when using the traditional approach. Therefore, the errors in the traditional method are attributed to both load and pure-fault current factors.
- Field Event 2 is from a single-circuit, homogenous 230 kV line which runs 153.17 km long with no taps. Compared to other events discussed in this paper, this event had relatively higher pre-fault I_2 and I_0 as percentages of I_1, measuring 6.33 percent and 0.77 percent respectively. The Z_{21} and Z_{20} estimations also showed higher magnitudes, making their inclusion crucial for this line. Although the pre-fault load current was not notably high, the fault-location estimation error using the traditional method was the highest among all the field events analyzed. This increased error could be attributed to pure-fault current-based errors, likely influenced by significant SIR differences, non-homogeneity, and asymmetry due to the fault location at 40 percent of the line length.

TABLE III
FIELD EVENTS FL ESTIMATION COMPARISON

Event	Fault Type	Pre-fault Seq. Currents $I_1/I_2/I_0$ (A Primary)	Line Parameters (Ohms Secondary and Deg.)		SIR (Angle = Deg.)		Actual Fault Loc. (km)	Traditional Approach		Proposed Approach Estimates and Error			
			Z_{1L}	Z_{0L}	$SIR_S = Z_{2S}/Z_{1L}$	$SIR_R = Z_{2R}/Z_{1L}$		FL Est. (km)	Error (km)	Z_{21} (Ohms Secondary and Deg.)	Z_{20} (Ohms Secondary and Deg.)	FL Est. (km)	Error (km)
1	BG	529.3 /21 /0.9	3.17 ∠77.3	10.39 ∠72.49	0.35 ∠5.5	0.27 ∠–8.1	7.36	8.44	–1.08	0.3 ∠−105.6	0.2 ∠154	8.03	−0.67
2	CG	166 /10.5 /1.3	23.53 ∠71.71	46.6 ∠81.14	0.67 ∠17.2	1.21 ∠–3.9	61.50	63.11	–1.61	2 ∠−138.6	1.31 ∠100.5	61.74	−0.24
3	BG	105.5 /4.7 /0.8	5.22 ∠79.54	12.72 ∠75.74	0.68 ∠–1.9	0.49 ∠–4.4	33.87	34.26	–0.39	0.45 ∠48.8	0.16 ∠−136.6	34.06	−0.19
4	BG	46.3 /1.9 /0.2	5.22 ∠79.54	12.72 ∠75.74	0.764 ∠–3.9	0.46 ∠–5.5	29.04	29.66	–0.62	0.66 ∠59.5	0.47 ∠−150.6	29.06	−0.02
5	BG	91.4 /3.4 /0.9	5.22 ∠79.54	12.72 ∠75.74	0.94 ∠–4.9	0.47 ∠–3.8	59.43	58.85	0.58	0.47 ∠51	0.21 ∠−135.4	59.56	−0.13

Although pure-fault current may be the theoretical cause, this error could also be linked to practical factors such as CT or PT errors or an incorrect Z_{1L} entry. However, the exact cause remains uncertain. Theoretically, omitting Z_{21} and Z_{20} could have had a more significant impact on this event. If the fault had been further from the midpoint or if the pre-fault load had been higher, the errors from the traditional approach would have been even more pronounced.

- Field Events 3, 4, and 5 all occur on the same 220 kV line, which is a single-circuit homogeneous 61.987 km long line with no taps. Although these three field events occur on the same line, the Z_{21} and Z_{20} estimates show some variation. This variation could be due to changes in pre-fault sequence currents, which may affect CT errors.

Field Events 3 and 5 have similar levels of pre-fault currents, resulting in only minor variations in their Z_{21} and Z_{20} estimates. However, Field Event 4 has a low pre-fault current, leading to estimates that are comparatively off. These events highlight the importance of estimating Z_{21} and Z_{20} at higher load conditions, averaging these estimates over time, and storing them in the relay memory.

As seen from Table III, the proposed FL method consistently provides a more accurate fault-location estimate than the traditional method in all the field cases.

V. LIMITATIONS OF THE PROPOSED METHOD

The proposed FL method is a multiterminal method and therefore requires reliable communications channels and synchronized remote data. Consequently, it faces the same limitations as traditional multiterminal methods. Additionally, certain conditions can restrict the Z_{21} (19) and Z_{20} (20) estimation process and affect FL accuracy.

- Real-life errors such as incorrect Z_{1L} and Z_{0L}, as well as CT and PT errors, can impact the estimation of sequence-coupling line parameters with the proposed method, leading to reduced FL accuracy improvements.
- As discussed in Section III.C, Z_{21} and Z_{20} estimations have accuracy limitations. Furthermore, the proposed FL solution does not fully address all sequence mutual-coupling errors for double-circuit lines.
- Intermittently transposed lines behave like transposed lines under normal operating conditions, resulting in Z_{21} and Z_{20} estimations being zero. However, during fault conditions, these lines may exhibit untransposed errors depending on the fault location. The proposed method does not effectively handle these dynamic untransposed errors.

VI. CONCLUSION

Untransposed lines introduce mutual coupling in sequence networks; ignoring this effect in the negative-sequence network during FL can lead to significant errors. This paper analyzes the errors introduced by the traditional ME fault-location method and categorizes them as load-current-based errors and pure-fault current-based errors. Traditionally, sequence-coupling parameters are ignored, but the proposed FL algorithm includes them to enhance accuracy. Users do not need to input these additional parameters manually as the algorithm estimates them using pre-fault voltage and current data from both line ends. The paper also illustrates the improvements upon the Z_{20}

estimation for double-circuit lines so that the proposed method can be reliably applied to get accurate FL in end-to-end parallel lines. Extensive simulations and field tests demonstrate the effectiveness of the proposed algorithm, showing promising results in accurately locating faults.

VII. Appendix

The transmission line parameters for the five tower configurations we discussed in the paper are listed in Table IV and Table V.

TABLE IV
LINE PARAMETERS FOR 100 KM SINGLE-CIRCUIT AND DOUBLE-CIRCUIT OVERHEAD LINES WITH SOIL RESISTIVITY (RHO)=100 Ω-METER

Values–400 kV Horizontal Single-Circuit Configuration	
Z_{012} (Ω)	$\begin{bmatrix} 30.7409+87.4077i & 1.0162-0.8507i & -1.2448-0.4547i \\ -1.2448-0.4547i & 1.5893+31.7901i & -2.8321+1.8216i \\ 1.0162-0.8507i & 2.9936+1.5419i & 1.5893+31.7901i \end{bmatrix}$
Y_{012} (mSiemens)	$\begin{bmatrix} 0.3666i & -0.0125+0.0072i & 0.0125+0.0072i \\ 0.0125+0.0072i & 0.5286i & 0.0355-0.0205i \\ -0.0125+0.0072i & -0.0355-0.0205i & 0.5286i \end{bmatrix}$
Values–400 kV Vertical Single-Circuit Configuration	
Z_{012} (Ω)	$\begin{bmatrix} 26.36+103.41i & 1.8+0.63i & -2.81-0.11i \\ -2.81-0.11i & 1.47+27.69i & -2.99+1.65i \\ 1.8+0.63i & 3.02+1.56i & 1.47+27.69i \end{bmatrix}$
Y_{012} (mSiemens)	$\begin{bmatrix} 0.2457i & -0.0155+0.0115i & 0.0155+0.0115i \\ 0.0155+0.0115i & 0.5956i & 0.0631-0.0334i \\ -0.0155+0.0115i & -0.0631-0.0334i & 0.5956i \end{bmatrix}$
Values–230 kV Right Angle Single-Circuit Configuration	
Z_{012} (Ω)	$\begin{bmatrix} 27.83+122.13i & -1.52+1.56i & 1.28+1.115i \\ 1.28+1.115i & 3.47+38.89i & 3.44-2.333i \\ -1.52+1.56i & 3.45-2.34i & 3.47+38.89i \end{bmatrix}$
Y_{012} (mSiemens)	$\begin{bmatrix} 0.2543i & 0.0154-0.003i & -0.0154-0.003i \\ -0.0154-0.003i & 0.4277i & -0.0352+0.0241i \\ 0.0154-0.003i & 0.0352+0.0241i & 0.4277i \end{bmatrix}$
Values–400 kV Double-Circuit Configuration	
Z_{012} (Ω)	$1.0e+02 \bullet$ $\begin{bmatrix} 0.2589+1.0371i & 0.0233-0.0063i & -0.0152-0.0007i \\ 0.2442+0.6214i & 0.0052-0.0081i & \end{bmatrix}$ $\begin{bmatrix} -0.0152-0.0007i & 0.0152+0.2765i & -0.0292+0.0166i \\ 0.0039-0.0025i & 0.0011+0.0131i & \end{bmatrix}$ $\begin{bmatrix} 0.0233-0.0063i & 0.0302+0.0149i & 0.0152+0.2765i \\ 0.0052-0.0081i & 0.0111+0.0035i & \end{bmatrix}$ $\begin{bmatrix} 0.2442+0.6214i & 0.0052-0.0081i & 0.0039-0.0025i \\ 0.2589+1.0371i & 0.0233-0.0063i & \end{bmatrix}$ $\begin{bmatrix} 0.0039-0.0025i & 0.0011+0.0131i & -0.0100+0.0054i \\ -0.0152-0.0007i & 0.0152+0.2765i & \end{bmatrix}$
Y_{012} (mSiemens)	$\begin{bmatrix} 0.0000+0.2865i & -0.0193+0.0080i & 0.0193+0.0080i & -0.0000-0.1074i \\ 0.0089+0.0079i & -0.0089+0.0079i & & \end{bmatrix}$ $\begin{bmatrix} 0.0193+0.0080i & 0.0000+0.5975i & 0.0613-0.0331i & -0.0089+0.0079i \\ 0.0000-0.0210i & 0.0162-0.0039i & & \end{bmatrix}$ $\begin{bmatrix} -0.0193+0.0080i & -0.0613-0.0331i & -0.0000+0.5975i & 0.0089+0.0079i \\ -0.0162-0.0039i & -0.0000-0.0210i & & \end{bmatrix}$ $\begin{bmatrix} -0.0000-0.1074i & 0.0089+0.0079i & -0.0089+0.0079i & 0.0000+0.2865i \\ -0.0193+0.0080i & 0.0193+0.0080i & & \end{bmatrix}$ $\begin{bmatrix} -0.0089+0.0079i & -0.0000-0.0210i & 0.0162-0.0039i & 0.0193+0.0080i \\ 0.0000+0.5975i & 0.0613-0.0331i & & \end{bmatrix}$ $\begin{bmatrix} 0.0089+0.0079i & -0.0162-0.0039i & 0.0000-0.0210i & -0.0193+0.0080i \\ -0.0613-0.0331i & -0.0000+0.5975i & & \end{bmatrix}$
Values–230 kV Double-Circuit Configuration	
Z_{012} (Ω)	$1.0e+02 \bullet$ $\begin{bmatrix} 0.3047+1.2398i & 0.0222-0.0098i & -0.0133-0.0019i & 0.2690+0.7579i \\ 0.0139-0.0027i & -0.0016+0.0053i & & \end{bmatrix}$ $\begin{bmatrix} -0.0133-0.0019i & 0.0357+0.3554i & -0.0287+0.0177i & -0.0016+0.0053i \\ 0.0016+0.0147i & -0.0091+0.0077i & & \end{bmatrix}$ $\begin{bmatrix} 0.0222-0.0098i & 0.0299+0.0157i & 0.0357+0.3554i & 0.0139-0.0027i \\ 0.0109+0.0049i & 0.0016+0.0147i & & \end{bmatrix}$

	$\begin{bmatrix} 0.2690 + 0.7579i & 0.0139 - 0.0027i & -0.0016 + 0.0053i & 0.3047 + 1.2398i \\ 0.0222 - 0.0098i & -0.0133 - 0.0019i & & \end{bmatrix}$ $\begin{bmatrix} -0.0016 + 0.0053i & 0.0016 + 0.0147i & -0.0091 + 0.0077i & -0.0133 - 0.0019i \\ 0.0357 + 0.3554i & -0.0287 + 0.0177i & & \end{bmatrix}$ $\begin{bmatrix} 0.0139 - 0.0027i & 0.0109 + 0.0049i & 0.0016 + 0.0147i & 0.0222 - 0.0098i \\ 0.0299 + 0.0157i & 0.0357 + 0.3554i & & \end{bmatrix}$
Y_{012} (mSiemens)	$\begin{bmatrix} 0.0000 + 0.2679\text{i} & -0.0089 + 0.0137\text{i} & 0.0089 + 0.0137\text{i} & -0.0000 - 0.0775\text{i} \\ 0.0010 + 0.0051\text{i} & -0.0010 + 0.0051\text{i} & & \end{bmatrix}$ $\begin{bmatrix} 0.0089 + 0.0137\text{i} & 0.0000 + 0.4674\text{i} & 0.0363 - 0.0192\text{i} & -0.0010 + 0.0051\text{i} \\ 0.0000 - 0.0130\text{i} & 0.0085 - 0.0039\text{i} & & \end{bmatrix}$ $\begin{bmatrix} -0.0089 + 0.0137\text{i} & -0.0363 - 0.0192\text{i} & -0.0000 + 0.4674\text{i} & 0.0010 + 0.0051\text{i} \\ -0.0085 - 0.0039\text{i} & -0.0000 - 0.0130\text{i} & & \end{bmatrix}$ $\begin{bmatrix} 0.0000 - 0.0775\text{i} & 0.0010 + 0.0051\text{i} & -0.0010 + 0.0051\text{i} & 0.0000 + 0.2679\text{i} \\ -0.0089 + 0.0137\text{i} & 0.0089 + 0.0137\text{i} & & \end{bmatrix}$ $\begin{bmatrix} -0.0010 + 0.0051\text{i} & -0.0000 - 0.0130\text{i} & 0.0085 - 0.0039\text{i} & 0.0089 + 0.0137\text{i} \\ 0.0000 + 0.4674\text{i} & 0.0363 - 0.0192\text{i} & & \end{bmatrix}$ $\begin{bmatrix} 0.0010 + 0.0051\text{i} & -0.0085 - 0.0039\text{i} & 0.0000 - 0.0130\text{i} & -0.0089 + 0.0137\text{i} \\ -0.0363 - 0.0192\text{i} & 0.0000 + 0.4674\text{i} & & \end{bmatrix}$

TABLE V
TOWER CONFIGURATION DATA FOR THE LINES DISCUSSED (AS ENTERED IN ATP DRAW)

400 kV Horizontal Tower Configuration Data

Parameter / Condition	Ph.no.	Rin (cm)	Rout (cm)	Resistivity (Ω/km Double Circuit)	Horizontal (m)	Vtower (m)	Vmid (m)	Separation (cm)	Alpha (degree)	NB
1	1	0	1.5885	0.0547	0	21.798	8.84	45.2547	45	4
2	2	0	1.5885	0.0547	11	21.798	8.84	45.2547	45	4
3	3	0	1.5885	0.0547	22	21.798	8.84	45.2547	45	4
4	0	0	0.412	0.8525	2.97	29.27	17.27	0	0	1
5	0	0	0.412	0.8525	19.03	29.27	17.27	0	0	1

400 kV Vertical Tower Configuration Data

Parameter / Condition	Ph.no.	Rin (cm)	Rout (cm)	Resistivity (Ω/km Double Circuit)	Horizontal (m)	Vtower (m)	Vmid (m)	Separation (cm)	Alpha (degree)	NB
1	1	0	1.5885	0.0547	0	28.2002	18.8001	45.2547	45	4
2	2	0	1.5885	0.0547	0.6	36.2001	24.1341	45.2547	45	4
3	3	0	1.5885	0.0547	2.22	44.2001	29.4682	45.2547	45	4
4	0	0	0.412	0.8525	4.0996	60.0002	40.0001	0	0	1
5	0	0	0.412	0.8525	10.8997	60.0002	40.0001	0	0	1

230 kV Right Angle Tower Configuration Data

Parameter / Condition	Ph.no.	Rin (cm)	Rout (cm)	Resistivity (Ω/km Double Circuit)	Horizontal (m)	Vtower (m)	Vmid (m)	Separation (cm)	Alpha (degree)	NB
1	1	0	1.43	0.0674	0	19.6292	10.7107	28.9999	0	2
2	2	0	1.43	0.0674	12.6005	19.6292	10.7107	28.9999	0	2
3	3	0	1.43	0.0674	0.3505	25.3302	16.4105	28.9999	0	2
4	0	0	0.412	0.8525	6.3002	37.6307	33.0313	0	0	1

400 kV Double-Circuit Tower Configuration Data

Parameter / Condition	Ph.no.	Rin (cm)	Rout (cm)	Resistivity (Ω/km Double Circuit)	Horizontal (m)	Vtower (m)	Vmid (m)	Separation (cm)	Alpha (degree)	NB
1	1	0	1.5885	0.0547	0	28.2002	18.8001	45.2547	45	4
2	2	0	1.5885	0.0547	0.6	36.2001	24.1341	45.2547	45	4
3	3	0	1.5885	0.0547	2.22	44.2001	29.4682	45.2547	45	4
4	4	0	1.5885	0.0547	15	28.2002	18.8001	45.2547	45	4
5	5	0	1.5885	0.0547	14.4	36.2001	24.1341	45.2547	45	4
6	6	0	1.5885	0.0547	12.78	44.2001	29.4682	45.2547	45	4
7	0	0	0.412	0.8525	4.0996	60.0002	40.0001	0	0	1
8	0	0	0.412	0.8525	10.8997	60.0002	40.0001	0	0	1

230 kV Double-Circuit Tower Configuration Data

Parameter / Condition	Ph.no.	Rin (cm)	Rout (cm)	Resistivity (Ω/km Double Circuit)	Horizontal (m)	Vtower (m)	Vmid (m)	Separation (cm)	Alpha (degree)	NB
1	1	0	1.43	0.0674	0	14.985	7.015	28.9999	0	2
2	2	0	1.43	0.0674	0	20.0851	12.1149	28.9999	0	2
3	3	0	1.43	0.0674	0	25.1857	17.2152	28.9999	0	2
4	4	0	1.43	0.0674	9.7399	14.985	7.015	28.9999	0	2
5	5	0	1.43	0.0674	9.7399	20.0851	12.1149	28.9999	0	2
6	6	0	1.43	0.0674	9.7399	25.1857	17.2152	28.9999	0	2
7	0	0	0.412	0.8525	4.87	30.8312	22.8601	0	0	1

Appendix A: Derivation for $Z_{20} = Z_{01}$

We know that the relation between sequence impedance matrix and phase impedance matrix is as shown below,

$$\mathrm{Z}_{012} = A \bullet Z_{abc} \bullet A^{-1} \tag{29}$$

Where:

$A = \frac{1}{3}\begin{bmatrix} 1 & 1 & 1 \\ 1 & \alpha & \alpha^2 \\ 1 & \alpha^2 & \alpha \end{bmatrix}$, and $\alpha = 1\angle 120^0$

When we substitute A Matrix in (29) and expand the matrices as shown below,

$$\begin{bmatrix} Z_{00} & Z_{01} & Z_{02} \\ Z_{10} & Z_{11} & Z_{12} \\ Z_{20} & Z_{21} & Z_{22} \end{bmatrix} = \frac{1}{3} \bullet \begin{bmatrix} 1 & 1 & 1 \\ 1 & \alpha & \alpha^2 \\ 1 & \alpha^2 & \alpha \end{bmatrix} \bullet \begin{bmatrix} Z_{aa} & Z_{ab} & Z_{ac} \\ Z_{ba} & Z_{bb} & Z_{bc} \\ Z_{ca} & Z_{cb} & Z_{cc} \end{bmatrix} \bullet \begin{bmatrix} 1 & 1 & 1 \\ 1 & \alpha^2 & \alpha \\ 1 & \alpha & \alpha^2 \end{bmatrix}$$

From the above equation, we can write,

$$\begin{aligned} \mathrm{Z}_{01} = \frac{1}{3} \bullet [&(Z_{aa} + Z_{ba} + Z_{ca}) \\ &+\alpha^2(Z_{ab} + Z_{bb} + Z_{cb}) \\ &+\alpha(Z_{ac} + Z_{bc} + Z_{cc}) \end{aligned} \tag{30}$$

And

$$\begin{aligned} \mathrm{Z}_{20} = \frac{1}{3} \bullet [&(Z_{aa} + \alpha^2 Z_{ba} + \alpha Z_{ca}) \\ &+(Z_{ab} + \alpha^2 Z_{bb} + \alpha Z_{cb}) \\ &+(Z_{ac} + \alpha^2 Z_{bc} + \alpha Z_{cc}) \end{aligned} \tag{31}$$

We can apply the following relations in (30) and (31), rewriting $Z_{ab} = Z_{ba}$; $Z_{bc} = Z_{cb}$; $Z_{ca} = Z_{ac}$.

We get (32):

$$\begin{aligned} \mathrm{Z}_{01} = \frac{1}{3} \bullet [&(Z_{aa} + Z_{ab} + Z_{ac}) \\ &+\alpha^2(Z_{ba} + Z_{bb} + Z_{bc}) \\ &+\alpha(Z_{ca} + Z_{cb} + Z_{cc}) \end{aligned} \tag{32}$$

In Equation (31) and (32), the right-hand-side terms are the same; hence, we get:

$$\mathrm{Z}_{20} = Z_{01}$$

Appendix B: Derivation for Proposed Fault-Locating Equation Using Sequence Mutual-Coupling Parameters

We can write the negative-sequence network equation for the faulted condition from Fig. 5:

$$\begin{aligned}\mathrm{V_{2Sf}} - \mathrm{V_{2Rf}} = {} & \mathrm{m} \bullet \mathrm{Z_{22}} \bullet \mathrm{I_{2Sf}} + \mathrm{m} \bullet \mathrm{Z_{21}} \bullet \mathrm{I_{1Sf}} + \mathrm{m} \bullet \mathrm{Z_{20}} \bullet \mathrm{I_{0Sf}} \\ & - (1 - \mathrm{m}) \bullet \mathrm{Z_{22}} \bullet \mathrm{I_{2Rf}} - (1 - \mathrm{m}) \bullet \mathrm{Z_{21}} \\ & \bullet \mathrm{I_{1Rf}} - (1 - \mathrm{m}) \bullet \mathrm{Z_{20}} \bullet \mathrm{I_{0Rf}}\end{aligned}$$

$$\begin{aligned}\mathrm{V_{2Sf}} - \mathrm{V_{2Rf}} = {} & \mathrm{m} \bullet \mathrm{Z_{22}} \bullet (\mathrm{I_{2Sf}} + \mathrm{I_{2Rf}}) + \mathrm{m} \bullet \mathrm{Z_{21}} \bullet (\mathrm{I_{1Sf}} + \mathrm{I_{1Rf}}) \\ & + \mathrm{m} \bullet \mathrm{Z_{20}} \bullet (\mathrm{I_{0Sf}} + \mathrm{I_{0Rf}}) - \mathrm{Z_{22}} \bullet \mathrm{I_{2Rf}} - \mathrm{Z_{21}} \\ & \bullet \mathrm{I_{1Rf}} - \mathrm{Z_{20}} \bullet \mathrm{I_{0Rf}}\end{aligned}$$

Solving the above equation for m:

$$\mathrm{m} = \left(\frac{\mathrm{V_{2Sf}} - \mathrm{V_{2Rf}} + \mathrm{Z_{22}} \bullet \mathrm{I_{2Rf}} + \mathrm{Z_{21}} \bullet \mathrm{I_{1Rf}} + \mathrm{Z_{20}} \bullet \mathrm{I_{0Rf}}}{\mathrm{Z_{22}} \bullet (\mathrm{I_{2Sf}} + \mathrm{I_{2Rf}}) + \mathrm{Z_{21}} \bullet (\mathrm{I_{1Sf}} + \mathrm{I_{1Rf}}) + \mathrm{Z_{20}} \bullet (\mathrm{I_{0Sf}} + \mathrm{I_{0Rf}})} \right)$$

Appendix C: Proposed Approach—Effective Z_{21} for Parallel Lines

For parallel lines, we can write the pre-fault negative-sequence network equation (complete equation) as:

$$\begin{aligned}V_{2S-PRE} - V_{2R-PRE} = {} & \mathrm{Z_{20}} I_{0\mathrm{S-PRE}} \\ & + Z_{21} I_{1\mathrm{S-PRE}} + Z_{22} I_{2\mathrm{S-PRE}} \\ & + \mathrm{Z_{2-0P}} I_{0\mathrm{SP-PRE}} \\ & + Z_{2-1\mathrm{P}} I_{1\mathrm{SP-PRE}} + Z_{2-2\mathrm{P}} I_{2\mathrm{SP-PRE}}\end{aligned}$$

Ignoring the protected-line's zero-sequence coupling and the parallel line's negative and zero-sequence-coupling terms, we get (33).

$$\begin{aligned}& V_{2S-PRE} - V_{2R-PRE} \\ & = Z_{21} I_{1\mathrm{S-PRE}} + Z_{22} I_{2\mathrm{S-PRE}} \\ & \quad + Z_{2-1\mathrm{P}} I_{1\mathrm{SP-PRE}} \\ & = Z_{21-\mathrm{eff}} I_{1\mathrm{S-PRE}} + Z_{22} I_{2\mathrm{S-PRE}}\end{aligned} \tag{33}$$

We can write $Z_{21-\mathrm{eff}} I_{1\mathrm{S-PRE}} = Z_{21} I_{1\mathrm{S-PRE}} + Z_{2-1\mathrm{P}} I_{1\mathrm{SP-PRE}}$ for an end-to-end parallel line, we can assume $I_{1\mathrm{S-PRE}} = I_{1\mathrm{SP-PRE}}$.

Hence, we get $Z_{21-\mathrm{eff}} = Z_{21} + Z_{2-1\mathrm{P}}$.

Appendix D: Equation (25)—Effective Z_{01} for Parallel Lines:

For parallel lines, we can write the pre-fault zero-sequence network equation (complete equation) as follows:

$$\begin{aligned}V_{0S-PRE} - V_{0R-PRE} & \\ = \mathrm{Z_{00}} I_{0\mathrm{S-PRE}} + Z_{01} I_{1\mathrm{S-PRE}} + Z_{02} I_{2\mathrm{S-PRE}} & \\ + \mathrm{Z_{0-0P}} I_{0\mathrm{SP-PRE}} + Z_{0-1\mathrm{P}} I_{1\mathrm{SP-PRE}} & \\ + Z_{0-2\mathrm{P}} I_{2\mathrm{SP-PRE}} &\end{aligned}$$

Ignoring the protected-line's negative-sequence coupling and the parallel line's negative and zero-sequence-coupling terms (and $\mathrm{Z_{0-0P}} = Z_{0M}$), we get (34).

$$\begin{aligned}& V_{0S-PRE} - V_{0R-PRE} \\ & = Z_{00} I_{0\mathrm{S-PRE}} + Z_{01} I_{1\mathrm{S-PRE}} + \mathrm{Z_{0M}} I_{0\mathrm{SP-PRE}} \\ & \quad + Z_{0-1\mathrm{P}} I_{1\mathrm{SP-PRE}} \\ & = Z_{01-\mathrm{eff}} I_{1\mathrm{S-PRE}} + Z_{00} I_{0\mathrm{S-PRE}} \\ & \quad + \mathrm{Z_{0M}} I_{0\mathrm{SP-PRE}}\end{aligned} \tag{34}$$

We can write $Z_{01-\mathrm{eff}} I_{1\mathrm{S-PRE}} = Z_{01} I_{1\mathrm{S-PRE}} + Z_{0-1\mathrm{P}} I_{1\mathrm{SP-PRE}}$ for an end-to-end parallel line, and we can assume $I_{1\mathrm{S-PRE}} = I_{1\mathrm{SP-PRE}}$.

Hence, we get $Z_{01-\mathrm{eff}} = Z_{01} + Z_{0-1\mathrm{P}}$.

Appendix E: Equation (20)—Effective Z_{01} for Parallel Lines:

When we apply the same approach for (20), (which excludes the $\mathrm{Z_{0M}}$ term), we get (35).

$$V_{0S-PRE} - V_{0R-PRE} = Z_{00} I_{0\mathrm{S-PRE}} + Z_{01} I_{1\mathrm{S-PRE}} \tag{35}$$

When we compare the right-hand side terms in (34) and (35) and cancel all the same terms, $\mathrm{Z_{01}}$ effectively, in (35), is as follows:

$$Z_{01-\mathrm{eff}} = Z_{01} + \mathrm{Z_{0-1P}} + \frac{\mathrm{Z_{0M}} I_{0\mathrm{SP-PRE}}}{I_{1\mathrm{S-PRE}}}$$

Appendix F: Equation (15), (16), and (17)—Effective Y_{x1} for Parallel Lines (Where X = 0, 1, 2)

From Equation (14):

$$\begin{aligned}I_{xS-PRE} + I_{xR-PRE} & \\ = k_{1S} \bullet Y_{x1} \bullet V_{1S-PRE} + k_{1R} \bullet Y_{x1} \bullet V_{1R-PRE} & \\ + k_{1SP} \bullet Y_{x-1P} \bullet V_{1SP-PRE} + k_{1RP} \bullet Y_{x-1P} & \\ \bullet V_{1RP-PRE} &\end{aligned}$$

For the end-to-end parallel lines:

$$\begin{aligned}V_{1SP-PRE} &= V_{1S-PRE} \\ k_{1SP} &= k_{1S} \\ k_{1RP} &= k_{1R}\end{aligned}$$

Hence, the above equation turns out to be (36):

$$\begin{aligned}& I_{xS-PRE} + I_{xR-PRE} \\ & = k_{1S} \bullet Y_{x1-eff} \bullet V_{1S-PRE} + k_{1R} \bullet Y_{x1-eff} \bullet V_{1R-PRE}\end{aligned} \tag{36}$$

Where:

$$Y_{x1-eff} = Y_{x1} + Y_{x-1P}.$$

Appendix G: Derivation for List of Errors in the Traditional Approach for Parallel Lines

The sequence network equation for a parallel line is shown in the following equation:

$$\begin{bmatrix} V_{0S}-V_{0R} \\ V_{1S}-V_{1R} \\ V_{2S}-V_{2R} \\ V_{0SP}-V_{0RP} \\ V_{1SP}-V_{1RP} \\ V_{2SP}-V_{2RP} \end{bmatrix} = \begin{bmatrix} Z_{00} & Z_{01} & Z_{02} & Z_{0-0P} & Z_{0-1P} & Z_{0-2P} \\ Z_{10} & Z_{11} & Z_{12} & Z_{1-0P} & Z_{1-1P} & Z_{1-2P} \\ Z_{20} & Z_{21} & Z_{22} & Z_{2-0P} & Z_{2-1P} & Z_{2-2P} \\ Z_{0P-0} & Z_{0P-1} & Z_{0P-2} & Z_{00} & Z_{01} & Z_{02} \\ Z_{1P-0} & Z_{1P-1} & Z_{2P-2} & Z_{10} & Z_{11} & Z_{12} \\ Z_{2P-0} & Z_{2P-1} & Z_{2P-2} & Z_{20} & Z_{21} & Z_{22} \end{bmatrix} \begin{bmatrix} I_{0S} \\ I_{1S} \\ I_{2S} \\ I_{0SP} \\ I_{1SP} \\ I_{2SP} \end{bmatrix}$$

The complete faulted negative-sequence network equation is shown in (37) (including superposition theorem):

$$\begin{aligned} V_{2Sf}-V_{2Rf} = {} & \mathrm{m}Z_{20}(I_{0S-FLT}+\mathrm{I}_{0S-PRE}) \\ & +\mathrm{m}Z_{21}(I_{1S-FLT}+\mathrm{I}_{1S-PRE}) \\ & +\mathrm{m}Z_{22}(I_{2S-FLT}+\mathrm{I}_{2S-PRE}) \\ & +\mathrm{m}Z_{2-0P}(I_{0SP-FLT}+\mathrm{I}_{0SP-PRE}) \\ & +\mathrm{m}Z_{2-1P}(I_{1SP-FLT}+\mathrm{I}_{1SP-PRE}) \\ & +\mathrm{m}Z_{2-2P}(I_{2SP-FLT}+\mathrm{I}_{2SP-PRE}) \\ & -(1-\mathrm{m})Z_{20}(I_{0R-FLT}+\mathrm{I}_{0R-PRE}) \\ & -(1-\mathrm{m})Z_{21}(I_{1R-FLT}+\mathrm{I}_{1R-PRE}) \\ & -(1-m)Z_{22}(I_{2R-FLT}+I_{2R-PRE}) \\ & -(1-\mathrm{m})Z_{2-0P}(I_{0RP-FLT}+\mathrm{I}_{0RP-PRE}) \\ & -(1-\mathrm{m})Z_{2-1P}(I_{1RP-FLT}+\mathrm{I}_{1RP-PRE}) \\ & -(1-\mathrm{m})Z_{2-2P}(I_{2RP-FLT}+\mathrm{I}_{2RP-PRE}) \end{aligned} \quad (37)$$

However, the traditional approach follows the transposed approach, as shown in (4). Hence, (38) provides a list of errors for the traditional approach for parallel lines.

1. $Z_{21} \bullet [\mathrm{m} \bullet I_{1S-FLT} - (1-\mathrm{m}) \bullet I_{1R-FLT}]$
2. $Z_{21} \bullet [\mathrm{m} \bullet I_{1S-PRE} - (1-\mathrm{m}) \bullet I_{1R-PRE}]$
3. $Z_{2-1P} \bullet [\mathrm{m} \bullet I_{1SP-FLT} - (1-\mathrm{m}) \bullet I_{1RP-FLT}]$
4. $Z_{2-1P} \bullet [\mathrm{m} \bullet I_{1SP-PRE} - (1-\mathrm{m}) \bullet I_{1RP-PRE}]$
5. $Z_{20} \bullet [\mathrm{m} \bullet I_{0S-FLT} - (1-\mathrm{m}) \bullet I_{0R-FLT}]$
6. $Z_{20} \bullet [\mathrm{m} \bullet I_{0S-PRE} - (1-\mathrm{m}) \bullet I_{0R-PRE}]$
7. $Z_{2-0P} \bullet [\mathrm{m} \bullet I_{0SP-FLT} - (1-\mathrm{m}) \bullet I_{0RP-FLT}]$
8. $Z_{2-0P} \bullet [\mathrm{m} \bullet I_{0SP-PRE} - (1-\mathrm{m}) \bullet I_{0RP-PRE}]$
9. $Z_{2-2P} \bullet [\mathrm{m} \bullet I_{2SP-FLT} - (1-\mathrm{m}) \bullet I_{2RP-FLT}]$
10. $Z_{2-2P} \bullet [\mathrm{m} \bullet I_{2SP-PRE} - (1-\mathrm{m}) \bullet I_{2RP-PRE}]$ (38)

The following assumption, (39), can be used for simplification.

$$\begin{aligned} I_{1S-PRE} &= -I_{1R-PRE} \\ I_{1SP-PRE} &= -I_{1RP-PRE} \\ I_{0SP-FLT} &= -I_{0RP-FLT} \\ I_{1SP-FLT} &= -I_{1RP-FLT} \\ I_{2SP-FLT} &= -I_{2RP-FLT} \end{aligned} \quad (39)$$

Applying (39) on the errors listed in (38), can simplify the traditional approach errors list for parallel lines, and results in List 1 provided in the Section II.B.

Appendix H: Derivation for List of Errors in the Proposed Approach Using Faulted Negative-Sequence Network for Parallel Lines

Fig. 14 provides the effective faulted negative-sequence network, when the Z_{21} and Z_{01} (= Z_{20}) estimations are done using (19) and (25), respectively. Network equations for Fig. 14, are given in the following,

$$\begin{aligned} V_{2Sf}-V_{2Rf} = {} & \mathrm{m}((Z_{20}+Z_{2-0P})I_{0Sf}+(Z_{21}+Z_{21-P})\,I_{1Sf} \\ & +Z_{22}I_{2Sf}) \\ & -(1-\mathrm{m})((Z_{20}+Z_{2-0P})I_{0Rf}+(Z_{21}+Z_{21-P})I_{1Rf} \\ & +Z_{22}I_{2Rf}) \end{aligned}$$

Using the superposition theorem, the above equation can be written as (40).

$$\begin{aligned} V_{2Sf}-V_{2Rf} = {} & \mathrm{m}Z_{20}(I_{0S-FLT}+\mathrm{I}_{0S-PRE}) \\ & +\mathrm{m}Z_{21}(I_{1S-FLT}+\mathrm{I}_{1S-PRE}) \\ & +\mathrm{m}Z_{22}(I_{2S-FLT}+\mathrm{I}_{2S-PRE}) \\ & +\mathrm{m}Z_{2-0P}(I_{0S-FLT}+\mathrm{I}_{0S-PRE}) \\ & +\mathrm{m}Z_{2-1P}(I_{1S-FLT}+\mathrm{I}_{1S-PRE}) \\ & -(1-\mathrm{m})Z_{20}(I_{0R-FLT}+\mathrm{I}_{0R-PRE}) \\ & -(1-\mathrm{m})Z_{21}(I_{1R-FLT}+\mathrm{I}_{1R-PRE}) \\ & -(1-m)Z_{22}(I_{2R-FLT}+I_{2R-PRE}) \\ & -(1-\mathrm{m})Z_{2-0P}(I_{0R-FLT}+\mathrm{I}_{0R-PRE}) \\ & -(1-\mathrm{m})Z_{2-1P}(I_{1R-FLT}+\mathrm{I}_{1R-PRE}) \end{aligned} \quad (40)$$

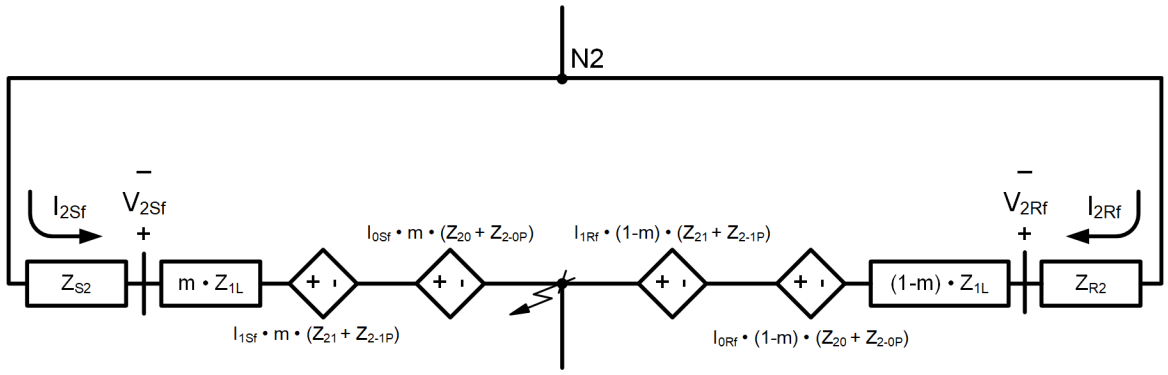

Fig. 14. Effective faulted negative-sequence network with proposed approach on parallel lines.

Comparing (37) and (40), and canceling the right-hand-side terms in both equations, the leftover terms are the errors.

Hence, (41) provides the list errors for the proposed approach.

1. $Z_{2-1P} \bullet [m \bullet I_{1S-FLT} - (1 - m) \bullet I_{1R-FLT}]$
2. $Z_{2-1P} \bullet [m \bullet I_{1S-PRE} - (1 - m) \bullet I_{1R-PRE}]$
3. $Z_{2-0P} \bullet [m \bullet I_{0S-FLT} - (1 - m) \bullet I_{0R-FLT}]$
4. $Z_{2-0P} \bullet [m \bullet I_{0S-PRE} - (1 - m) \bullet I_{1R-PRE}]$
5. $Z_{2-2P} \bullet [m \bullet I_{2S-FLT} - (1 - m) \bullet I_{2R-FLT}]$
6. $Z_{2-2P} \bullet [m \bullet I_{2S-PRE} - (1 - m) \bullet I_{2R-PRE}]$ (41)

Error 1 exists because $I_{1S\text{-}FLT}$ is not equal to $I_{1SP\text{-}FLT}$. Similarly, Error 3 exists because $I_{0S\text{-}FLT}$ is not equal to $I_{0SP\text{-}FLT}$.

Applying (39) to (41), the error terms can be written as shown in List 2, provided in the Section III.C.2.

VIII. Acknowledgment

The authors would like to express sincere appreciation for the technical support shared by engineers at Schweitzer Engineering Laboratories, Inc., including Emma Clawson, David Schmidt, Daqing Hou, Dale Finney, and Armando Guzmán, and extend their gratitude to Fernando Calero and Kanchanrao Dase for reviewing the paper.

IX. References

[1] S. Marx, B. Johnson, A. Guzmán, V. Skendzic, and V. Mynam, "Traveling-Wave Fault Location in Protective Relays: Design, Testing, and Results," proceedings of the 16th Annual Georgia Tech Fault and Disturbance Analysis Conference, Atlanta, GA, 2013.

[2] E. O. Schweitzer, A. Guzmán, M. V. Mynam, V. Skendzic, B. Kasztenny, and S. Marx, "Locating Faults by the Traveling Waves They Launch," 2014 67th Annual Conference for Protective Relay Engineers, College Station, Texas, 2014.

[3] B. Kasztenny, B. Le, and N. Fischer, "A New Multiterminal Fault-Location Algorithm Embedded in Line Current Differential Relays," proceedings of the 11th Annual International Conference on Development in Power System Protection, Birmingham, United Kingdom, 2012.

[4] D. Tziouvaras, J. Roberts, and G. Benmouyal, "New Multi-Ended Fault-Location Design for Two- or Three-Terminal Lines," proceedings of CIGRE Study Committee B5 Colloquium, Florence, Italy, 1999.

[5] O. Avendano, B. Kasztenny, HJ. Altuve, B. Le, and N. Fischer, "Tutorial on Fault Locating Embedded in Line Current Differential Relays–Methods, Implementation, and Application Considerations," Proceedings of the Annual Western Protective. Relay Conference, Spokane, Washington, 2014.

[6] P. Rithisha, O.D. Naidu, V. Pradhan, and N.V. Srikanth, "A Practical Methodology for Fault Location in Transmission Lines Without Line Parameter Settings and Data synchronization," Proceedings of the 17th International Conference on Developments in Power System Protection, Manchester, United Kingdom, 2024.

[7] A. Shrestha and S. K. Mutha, "New Multi-ended Fault-locating Method Utilizing Incremental Sequence Quantities," Proceedings of the 17th International Conference on Developments in Power System Protection, Manchester, United Kingdom, 2024.

[8] IEEE Std C37.114-2014, *IEEE Guide for Determining Fault Location on AC Transmission and Distribution Lines*.

[9] D. C. Deloach, J. D. Kuhlers, A. M. Murphy, and G. E. Piercy, "Voltage Unbalance in a Changing Grid," proceedings of the Annual Georgia Tech Fault and Disturbance Analysis Conference, Atlanta, Georgia, May 2022.

[10] G. Benmouyal and J. Roberts, "Superimposed Quantities: Their True Nature and Application in Relays," proceedings of the 26th Annual Western Protective Relay Conference, Spokane, WA, 1999.

[11] F. Calero, "Mutual Impedance in Parallel Lines–Protective Relaying and Fault-location Considerations," Proceedings of the 34th Annual Western Protective Relay Conference, Spokane, Washington, 2007.

[12] P. M. Anderson, *Analysis of Faulted Power Systems*, Vol. 11. John Wiley & Sons, Ames, Iowa, 1995.

[13] A. Shrestha and S. K. Mutha, "Transmission Line Parameter Estimation Using Traveling-Wave Fault-Location Data," proceedings of the 75th Annual Conference for Protective Relay Engineers, College Station, Texas, 2022.

X. Biographies

Sathish Kumar Mutha received his bachelor's degree in electrical and electronics engineering from Adam's Engineering College, Paloncha, India, in 2008 and his MS in electrical engineering from the University of North Carolina at Charlotte in 2020. Prior to earning his MS, he worked for more than nine years as an operations engineer in a coal-based power plant at Heavy Water Board, Dept of Atomic Energy, India. He joined Schweitzer Engineering Laboratories, Inc. (SEL) in 2019 as an engineer intern and currently holds a position of lead power engineer in the research and development division.

Arun Shrestha received his BSEE from the Institute of Engineering, at Pulchowk Lalitpur, Nepal, in 2005, and his MS and PhD in electrical engineering from the University of North Carolina at Charlotte in 2009 and 2016, respectively. He joined Schweitzer Engineering Laboratories, Inc. (SEL) in 2011 as an associate power engineer in research and development. He is presently working as a senior engineer. Arun holds six patents and has authored 17 technical papers. His research areas of interest include power system protection and control design, power system modeling and simulation, and digital substations. He is a senior member of IEEE and is a registered Professional Engineer. He is a member of IEEE PSRC and a US representative to IEC 61850 TC 57 WG.

Sajal Kumar Harmukh received his BTech degree in electrical power engineering in 2012 from the Indian Institute of Technology Delhi in India, and his MS degree in electrical engineering in 2016 from the University of Illinois at Urbana-Champaign. Previously, he worked for NTPC Limited, India, as an assistant manager in the operations and maintenance department. He currently works as a development lead power engineer at Schweitzer Engineering Laboratories, Inc.